The historical fingerprint and future impact of climate change on childhood malaria in Africa

Colin J. Carlson[1,2,*,†], Tamma A. Carleton[3,*], Romaric C. Odoulami[4], Cullen D. Molitor[5] and Christopher H. Trisos[4]

[1] *Department of Epidemiology of Microbial Diseases, Yale University School of Public Health*
[2] *Yale Center on Climate Change and Health, Yale University School of Public Health*
[3] *Department of Agricultural and Resource Economics, University of California, Berkeley*
[4] *African Climate and Development Initiative, University of Cape Town*
[5] *Bren School of Environmental Science & Management, University of California, Santa Barbara*
[*] *These authors share lead author status.*
[†] *Correspondence should be directed to colin.carlson@yale.edu.*

Submitted to *medRxiv* on August 6, 2024

Abstract

Health-related risks from climate change are growing exponentially[1], but direct attribution of health outcomes to human influence on the climate remains challenging[2,3]. Here, we leverage a comprehensive dataset of 50,425 population surveys[4] to investigate whether human-caused climate change has increased the burden of childhood malaria across sub-Saharan Africa. In historical data, we find that prevalence shows a robust response to temperature and extreme precipitation, consistent with expectations from previous empirical and epidemiological work. Comparing historical climate reconstructions to counterfactual simulations without anthropogenic climate forcings, we find two-to-one odds that human-caused climate change has increased the overall prevalence of childhood malaria across sub-Saharan Africa since 1901. We estimate that by 2014, human-caused climate change was responsible for an average of 87 excess cases of malaria per 100,000 children ages 2 to 10, with higher elevation and cooler regions in southern and east Africa experiencing greater increases. Under future climate change, we project that increasing temperatures could accelerate the elimination of malaria in west and central Africa, where the present-day burden is highest, with an average overall reduction of 94 (low greenhouse gas emissions, SSP1-RCP2.6) to 1,890 (high emissions, SSP5-RCP8.5) cases per 100,000 children in sub-Saharan Africa by the end of the century. However, we find that limiting future global warming to under 2°C (SSP1-RCP2.6) compared to 3°C (SSP2-RCP4.5) could prevent an average of 505 excess cases in southern Africa, and 33 excess cases in east Africa, per 100,000 children by 2100. Our study resolves a decades-old debate about one of the first suspected health impacts of climate change, and provides a template for future work measuring its true global burden.

Main Text

Despite progress towards global eradication, malaria remains the single deadliest climate-sensitive infectious disease[5]. Malaria transmission is highly responsive to temperature, driven by both the life cycle of the ectothermic mosquito vectors (*Anopheles* spp.) and the thermal sensitivity of the parasites (*Plasmodium* spp.) themselves[6,7]. In laboratory conditions, *P. falciparum* transmission by *An. gambiae* peaks around 25°C, and becomes negligible below ∼16°C or above ∼34°C[6,7,8]. Given these biological constraints, climate change has become a major concern for populations potentially at risk of malaria in southern and high-elevation east Africa, where temperatures may no longer be prohibitive to malaria transmission[9,10,11]. On the other hand, in west and central Africa—where the burden of malaria is highest—many studies suggest that climate change will reduce or eventually preclude transmission[9,10,12,13].

These risks were among the first proposed health impacts of climate change[14,15], but have been surprisingly contentious, and even described as "hot air"[16] and "dangerous pseudoscience"[17]. Malaria experts have often claimed that observed warming trends are incompatible with long-term reductions in malaria prevalence across Africa, and warned that other factors like drug resistance and funding instability pose a more serious threat to malaria eradication[16,18,19]. Empirical evidence to test these assumptions is sparse, with the highest profile studies focusing on a single dataset of malaria incidence over several decades at a tea plantation in Kericho, Kenya. Since 2000, over a dozen studies have argued that these data either support[20,21,22,23,24] or undermine[25,26,27,28,29,30,31] the broader hypothesis that climate change is responsible for a resurgence of malaria in the east African highlands[28,32,33,34,35]. More recently, a study by Snow *et al.*[4] examined the last century of continent-wide changes in malaria prevalence, and concluded that observed trends could not be neatly explained by climate change, but did so based only on visual correspondence between moving averages of rainfall, minimum temperature, and modeled malaria prevalence over the entire continent.

In this study, we revisit these debates by applying state-of-the-art methods from detection and attribution, an area of climate science that quantifies the historical and real-time climate impacts of anthropogenic greenhouse gas emissions[36,37]. These methods underpin the scientific consensus on human-caused climate change, and are regularly used to identify the role of climate change in the intensity, frequency, and distribution of specific extreme events (e.g., heatwaves, heavy precipitation, and droughts)[38,39,40]. However, attribution remains challenging for the downstream impacts of anthropogenic climate change on people and ecosystems, and methodological frameworks for impact attribution are still comparatively underdeveloped[3,41,42]. Applications to infectious disease dynamics are especially challenging, as relationships between climate and disease transmission are often complex, nonlinear, and confounded by human intervention, and few epidemiological datasets exist with sufficient spatial and temporal scope to resolve these relationships. As a result, hundreds of studies have tested for correlations between climate and observed changes in disease incidence or prevalence, but very few have shown that these changes are causally attributable to anthropogenic climate change[43,2].

Here, we draw on frameworks from climate science[38,39,40], econometrics[44,45], and epi-

demiology[43,2] to conduct an end-to-end impact attribution study (per[42]), measuring the direct effect of anthropogenic climate change on long-term trends in the burden of an infectious disease. We apply this framework to estimates of *falciparum* malaria prevalence in children aged 2-10 in sub-Saharan Africa ($Pf\mathrm{PR}_{2-10}$), which experiences roughly 95% of the global burden of malaria (with 80% of deaths in children under the age of 5)[46]. We analyze a recently published dataset with unparalleled resolution and scope (Figure 1), consisting of 50,425 surveys spanning more than a century (1900 to 2015)[4], which we aggregate to 9,875 monthly average values at the first administrative (state or province) level. Leveraging climate econometric methods[44,47,48], we develop a panel regression model that isolates the role of temperature and extreme precipitation from other confounding factors that also shape malaria endemicity (Figure 2; see Methods for details). Nonparametric controls in the model (i.e., fixed effects) account for regional differences in seasonality, time periods with concerted elimination efforts, and other spatiotemporal variation not explained by identifiable factors, such as socioeconomic or ecological differences between populations. To quantify statistical uncertainty in prevalence-climate relationships, we repeatedly estimate the model with 1,000 spatially-blocked bootstrapped samples. We apply these models to make predictions based on 10 sets of paired historical climate simulations with and without anthropogenic climate forcing, and estimate the impact of anthropogenic climate change on malaria prevalence from 1901 to 2014 (Figure 3). Finally, we project how future climate change could further alter malaria prevalence between 2015 and 2100, based on three future climate change scenarios for low (SSP1-RCP2.6), intermediate (SSP2-RCP4.5), and high (SSP5-RCP8.5) future greenhouse gas concentrations (Figure 4).

A robust signal of climate sensitivity

Over the last century, the prevalence of childhood malaria has exhibited a strong concave relationship with temperature (Figure 2A). Closely aligning with theoretical expectations that *P. falciparum* transmission by *Anopheles gambiae* mosquitoes should peak around 25.6°C[6], observed values of $Pf\mathrm{PR}_{2-10}$ in our dataset peak around a monthly mean temperature of 25.8°C (Figure S1). Based on these biological expectations, we estimate the effect of temperature as a quadratic response in a panel regression model, and find that prevalence peaks at 24.9°C (95% confidence interval across the 1,000 bootstrapped models: 22.5°C, 27.0°C). These results confirm that laboratory-based studies approximate malaria epidemiology in real populations quite well, and that temperature plays a substantial role in transmission dynamics: a 10°C increase or decrease from the optimal temperature lowers prevalence by ∼8 percentage points.

The relationship between precipitation and malaria prevalence is more complex[49], and likely less consequential for historical trends (Figures 2B, 2C). Contemporaneous monthly precipitation exhibits a nonlinear, but highly uncertain, relationship to prevalence (see Figure S12). To parsimoniously capture nonlinear effects and disentangle divergent impacts of low and high precipitation, we define precipitation shocks with two binary indicator variables, equal to one when monthly precipitation falls below 10% (we label this a "drought shock") or above 90% ("flood shock") percentiles of monthly

precipitation calculated for each subnational unit. While drought and flood events are complex phenomena, which develop from the combination of multiple factors (e.g., soil conditions and topography) in addition to rainfall over varying timescales, we use this drought/flood terminology as shorthand to indicate extremely low or high precipitation months. Although most effects are statistically insignificant, we find that drought shocks tend to decrease malaria prevalence 1-2 months later, while conversely, flood shocks have a positive effect on prevalence 2-3 months later. These effects and their timing are broadly consistent with expectations about how precipitation mediates the availability of mosquito breeding habitat: dry-out kills larvae and eggs, while inundation creates new breeding habitat[50,51,52,53,54,55,56,57]. Sensitivity analyses were also weakly suggestive of another established mechanism, in which floods may wash away eggs and larvae, reducing transmission in the shorter term (see Figures S10 and S12). Overall, extreme precipitation has a measurable effect on malaria prevalence, but may be less important than temperature; however, given the sparsity of weather station data[58] and the uncertainty of precipitation reconstructions[59], it is also possible that our analysis unavoidably underestimates the effect of precipitation due to measurement error.

Additional sensitivity analyses reinforce that these prevalence-climate relationships are both statistically robust and biologically consistent. Key findings are generally insensitive to alternative model specifications, such as: the inclusion of lagged effects of temperature (Figure S7); higher-order polynomial effects of temperature (Figure S11); alternative definitions of drought and flood shocks (Figures S8-S10); and alternative spatiotemporal controls, which account differently for variation over space (at region, country, and state levels), time (including yearly and monthly variation), and interactions among space and time (Figure S6 and Table S2).

Historical impacts of climate change (1901-2014)

We find that anthropogenic climate change has, more likely than not, been responsible for a small increase in the average prevalence of childhood malaria across sub-Saharan Africa since 1901 (Figures 2D). Compared to counterfactual simulations without anthropogenic climate forcing, we estimate that by 2010-2014, anthropogenic climate change had caused an increase in continental mean $Pf\mathrm{PR}_{2-10}$ of 0.09 percentage points (*p.p.*; 95% confidence interval: -0.30 *p.p.*, 0.51 *p.p.*). Simulations with an attributable increase in continent-wide mean prevalence outnumber those with losses by two to one (proportion P_+ of 10,000 paired factual versus counterfactual simulations with a positive difference in prevalence = 0.66). These increases are almost entirely driven by rising temperatures from anthropogenic climate forcing; the effects of drought and flood events on prevalence show no distinguishable signal from anthropogenic climate forcing over time (Figure S4).

This overall trend masks substantial regional heterogeneity in historical climate change impacts (Figure 3A; Figure S2), driven almost entirely by elevational and latitudinal gradients in temperature (Figure 3B,C). For example, attributable changes in prevalence across southern Africa are high in both magnitude and certainty, with an overall increase of 0.63 *p.p.* (95% CI: -0.04 *p.p.*, 1.40 *p.p.*; $\mathrm{P}_+ = 0.97$)—nearly an order of magnitude greater than the continental mean. In contrast, climate change has contributed to signifi-

cantly lower malaria prevalence in west Africa (mean = -0.38 *p.p.*; 95% CI: -0.90 *p.p.*,0.02 *p.p.*; $P_+ = 0.03$), where temperatures already often exceed the biological optimum for transmission. In the central African basin, a stronghold of malaria endemicity with average temperatures close to the 25°C optimum, the change in prevalence attributable to anthropogenic climate change is positive, relatively small, and uncertain (mean = 0.18 *p.p.*; 95% CI: -0.19 *p.p.*, 0.61 *p.p.*; $P_+ = 0.83$). Finally, we estimate a meaningful overall increase in prevalence attributable to anthropogenic climate change in east Africa (mean = 0.33 *p.p.*; 95% CI: -0.14 *p.p.*, 0.87 *p.p.*; $P_+ = 0.91$), but note that changes in prevalence are distributed unevenly along the steep elevational gradient: increases of up to 1-2 *p.p.* in the Ethiopian highlands and the greater Rift Valley region are accompanied by small but significant local declines throughout lowland areas in Ethiopia, Sudan, South Sudan, Eritrea, and Djibouti.

While these effects are meaningful, we caution that they are also far smaller than the reduction achieved through healthcare, mosquito nets, vector control, and economic development: previous work with the same dataset has estimated a reduction since 1900 of 16 *p.p.* (that is, a continent-wide decline in average $Pf\mathrm{PR}_{2-10}$ from 40% in 1900-1929 to 24% by 2010-2015[4]), while our estimates of historical climate change-attributable changes rarely exceed 1.5 *p.p.* for any individual administrative region. Additionally, we estimate that average reductions in prevalence realized during the Global Malaria Eradication Program (1955-1969; estimated reduction averaged over the entire period: -4.80 *p.p.*) and recent programs like Roll Back Malaria and the Global Technical Strategy (2000–2014; estimated reduction averaged over the entire period: -3.35 *p.p.*) were substantially larger than the cumulative effects of anthropogenic climate change (Table S2). Relatively small and spatially differentiated climate-related changes in burden could have been easily concealed by the greater impact of these programs, highlighting both the success of elimination programs and the importance of using an empirical approach like ours to isolate the effect of climate from other co-evolving factors.

Future impacts of climate change (2015-2100)

Despite contemporary trends, we project that within the next quarter-century, anthropogenic climate change will begin to reduce the prevalence of *falciparum* malaria in sub-Saharan Africa (Figure 2D; Table S1). This trend is driven largely by rising temperatures in lowland areas north of the equator, with greater possible reductions in higher greenhouse gas emissions scenarios (Figure 4). In these scenarios, temperature-related declines are slightly offset by floods, which will become more frequent across Africa[36], although their impact on overall trends is trivial when compared to temperature (Figure S5). Even in a future low emissions scenario (SSP1-RCP2.6: average global warming across models of +1.8°C in 2048-2052; +1.9°C in 2096-2100), increases in prevalence due to historical anthropogenic climate change are projected to essentially be offset by mid-century, stabilizing around an -0.09 *p.p.* (95% CI: -0.41 *p.p.*, 0.17 *p.p.*) projected decline across sub-Saharan Africa, relative to 2015-2020. In a high emissions scenario (SSP5–RCP8.5: +2.4°C in 2048-2052; +5.2°C in 2096-2100), we project decreases in prevalence would accelerate over time, reaching an average of -0.24 *p.p.* (95% CI: -0.80

p.p., 0.26 *p.p.*) by mid-century, and -1.90 *p.p.* (95% CI: -4.85 *p.p.*, -0.07 *p.p.*) by the end of the century—a projected reduction that begins to approach the magnitude of some historical eradication programs.

Though the balance across regions will begin to shift, the geographic pattern of future changes in malaria prevalence is likely to reproduce present-day heterogeneity in impacts, as malaria transmission continues to shift along latitudinal and elevational clines in temperature (Figure 4; Figure S3). West Africa is projected to experience the most dramatic transformation, especially in a high-emissions scenario (SSP5-RCP8.5), with a projected decline of -1.04 *p.p.* (95% CI: -1.86 *p.p.*, -0.36 *p.p.*) by mid-century, and a staggering -4.25 *p.p.* (95% CI: -8.78 *p.p.*, -1.52 *p.p.*) decrease by 2100. Similar but shallower declines are projected in central Africa, where end-of-century reductions could reach between -0.06 *p.p.* (SSP1-RCP2.6; 95% CI: -0.43 *p.p.*, 0.24 *p.p.*) and -1.43 *p.p.* (SSP5-RCP8.5; 95% CI: -4.36 *p.p.*, 0.37 *p.p.*). On the other hand, localized increases in prevalence will continue in the cooler parts of the Ethiopian highlands, the greater Rift Valley region, and coastal southern Africa, potentially reaching 5 *p.p.* or more in some areas. The overall effect across east and southern Africa is a projected increase in prevalence, except in the highest emissions scenario (SSP5-RCP8.5), where both regions start to experience declines by mid-century, with east Africa eventually falling -0.60 *p.p.* (95% CI: -2.72 *p.p.*, 0.95 *p.p.*) below present-day levels by 2100.

Broadly, our results suggest that the main effect of climate change mitigation will be to keep average temperatures in sub-Saharan Africa closer to the optimum range for malaria transmission. However, for many cooler localities, such as in east and southern Africa, greenhouse gas emissions reductions would prevent substantial climate change-driven increases in malaria prevalence. By mid-century, limiting global warming to below the +2°C limit in the Paris Agreement (achieved under SSP1-RCP2.6) is projected to prevent an estimated 163 cases of malaria per 100,000 children in southern Africa and 20 cases per 100,000 children in east Africa compared to an intermediate emissions scenario (SSP2-RCP4.5: +2.0°C in 2048-2052; +3.0°C in in 2096-2100). By the end of the century, these benefits would be even greater, with 505 and 33 excess cases averted per 100,000 children in southern and east Africa, respectively (Table S1). At a more local scale, these benefits could be at least an order of magnitude greater (Figure S3).

Discussion

In this study, we apply an end-to-end impact attribution framework to a century of malaria surveillance, allowing us to estimate the historical and projected future impact of anthropogenic climate change on childhood malaria in sub-Saharan Africa. We find a 66% likelihood that anthropogenic climate change since 1901 has increased malaria burden; on average across Africa, an estimated 87 excess malaria cases per 100,000 people can be attributed to historical human-caused climate change. However, this burden falls disproportionately on southern and east Africa; we estimate a 97% and 91% likelihood, respectively, that anthropogenic climate change has increased present-day malaria prevalence in these regions. We project that prevalence in both southern and east Africa will remain elevated in the future: even in a low emissions scenario likely to limit global

warming below +2°C (SSP1-RCP2.6), we estimate these regions will face 339 and 98 excess cases of malaria per 100,000 children by 2100, respectively. In contrast, across many other regions of Africa, we project that the overall impact of future climate change will be a net reduction in malaria: these changes are projected to be most dramatic in west and central Africa, where future climate change could reduce prevalence by up to ∼4,200 (west Africa) and ∼1,400 (central Africa) cases per 100,000 children in a high-emissions scenario (SSP5-RCP8.5). Our results suggest that climate change could be synergistic with eradication efforts in countries like Nigeria and the Democratic Republic of the Congo, where the present-day burden of malaria is highest, but will continue to create new risks in countries like Ethiopia and South Africa.

Spanning multiple centuries, our analysis is the most comprehensive look to date at the impact of climate change on any infectious disease, and brings new clarity to a decades-long debate in malaria research. Whereas some work has questioned the plausibility that overall declines in continent-wide prevalence would conceal a climate-linked increase[4,19], the 0.087 percentage point increase in $Pf\mathrm{PR}_{2-10}$ that we attribute to historical anthropogenic climate change could easily be masked by the nearly 200-fold greater overall reduction observed across sub-Saharan Africa over the same period. Our regional estimates also generally align with previous lab-based or site-specific empirical work, which suggests that east and southern Africa are experiencing shifts towards temperatures that are permissive to transmission for the first time or over longer seasons[9,10], while in west and central Africa, climate change impacts have been harder to detect, and future warming might exceed the physiological limits of malaria transmission[9,10,13,60]. Notably, our study does provide robust, empirical evidence that human-caused climate change has at least marginally contributed to malaria resurgence in high-altitude Kenya and Ethiopia, consistent with local epidemic time series or simulated dynamics based on local weather station data[21,24,34].

Our study therefore reconciles three long-standing ideas that are sometimes treated as paradoxical: anthropogenic climate change is not the primary force shaping past, or probably future, trends in malaria prevalence[4,16,19]. However, anthropogenic climate change has increased the burden of malaria in sub-Saharan Africa[14,15,21,24], and at high elevations and latitudes, will continue to for several more decades[9,10]. Nevertheless, rising temperatures at lower latitudes and elevations in Africa will mostly align with future efforts to eradicate *Plasmodium falciparum* from sub-Saharan Africa[10,19,60].

In spite of climate change, elimination campaigns have already achieved substantial reductions in malaria endemicity over the last century. This history underscores the value of disease surveillance, healthcare, and vector control as core components of climate change adaptation, as well as the plausibility of malaria eradication within a generation[61]—a point echoed by the recent work on the elimination of malaria from Hainan Island in China[62]. At the same time, several recent anecdotes have raised relevant concerns about the fragility of elimination, such as the resurgence of malaria in Ecuador and Peru associated with migration from Venezuela[63], or the estimated 10,000 excess deaths due to malaria – and 3.5 million untreated cases – caused by healthcare disruptions during the 2014 Ebola virus epidemic in West Africa[64]. Concerns about

climate-linked resurgence are also more credible given the ongoing invasion of the *An. stephensi* mosquito, which thrives in cities, has already been reported in several locations in east Africa, and may be able to transmit *P. falciparum* up to much higher temperatures ($\sim$37°C) than *An. gambiae* can ($\sim$30°C)[8,65]. If *An. stephensi* were to become a dominant vector across the continent, climate change might become an even more pressing concern[66,67]. These risks only add more urgency to the global goals of eliminating both malaria and greenhouse gas emissions.

Methods

Malaria prevalence data

We use a recently published database of *Plasmodium falciparum* clinical prevalence in Sub-Saharan Africa[4]. This compendium, compiled by Snow *et al.* over more than two decades, is one of the most spatially and temporally complete publicly-available databases of infectious disease burden. The database covers the period from 1900 to 2015, though sampling has increased substantially since the turn of the century (pre-2000: $n = 32,533$; post-2000: $n = 17,892$). Most prevalence surveys used microscopy for diagnostics ($n = 36,805$) but a substantial portion of data also derive from rapid diagnostic tests ($n = 11,154$). The data have been compiled from a mix of archival research through public health documents, including the records of colonial governments and elimination campaigns from different periods; national survey data; electronic records published in peer-reviewed journals and grey data sources (e.g., World Health Organization technical documents); and a mix of other sources compiled by international organizations. Records were georeferenced in the original study using a standard set of protocols, with a 5km grid uncertainty threshold for point data, and broader areas stored as administrative polygons. In total, the data include a total of 50,425 prevalence surveys at a total of 36,966 unique georeferenced locations.

For our models, we used the estimates of malaria prevalence for children aged two to ten years old, as *falciparum* malaria has the highest mortality in children and pregnant women. The Snow *et al.* data cover all available prevalence surveys, including all age ranges, but were converted by the authors of the original study to a standardized estimate of prevalence in children aged 2-10 ($Pf\mathrm{PR}_{2-10}$), using a catalytic conversion Muench model. For our model, we aggregated data by averaging $Pf\mathrm{PR}_{2-10}$ at the first administrative level within-country (i.e., state or province level, or as shorthand, ADM1), using shapefiles provided by the Database of Global Administrative Areas dataset version 3.6 (www.gadm.org). This provided sufficient granularity to capture climate impacts and local heterogeneity in confounders, while ensuring sufficient data coverage within these units. This aggregation scale is supported by previous work that models this dataset at the same spatial resolution[4].

Climate data

We used two sets of climate data in this study. The first is an observational dataset from the Climatic Research Unit (hereafter, CRU-TS; version 4.03 for model training and bias correction), which is constructed from monthly observations from extensive networks of meteorological stations from around the globe[68]. CRU-TS provides land-only climatic variables at a high spatial resolution of $0.5^\circ \times 0.5^\circ$ extending from 1901 to present (though our analysis is limited to the period 1901-2014). The second set of data is from ten global climate models (GCMs) selected from the sixth phase of the Coupled Model Intercomparison Project (CMIP6). In our historical analysis, we analysed (per GCM) one model realization of the "Historical" simulation, which includes anthropogenic

greenhouse gas emissions, and one realization from the "Historical-Natural" simulation, which includes only solar and volcanic climate forcing. For both the Historical and Historical-Natural (hereafter and in the main text, "historical climate" and "historical counterfactual") simulations, we analysed the period 1901-2014.

To investigate the continued effect of climate change on malaria prevalence between 2015 and 2100, we analysed three CMIP6 future climate change simulations from each of the 10 GCMs. Shared socio-economic pathways (SSPs) refer to the level of potential future global development (social, economic, and technological) and the implication for climate change mitigation and/or adaptation actions or policy[69,70]. SSPs are combined with various possible future radiative forcings (representative concentration pathways; RCPs) to form the climate change scenarios used in CMIP6. Of the available SSP–RCP scenarios, we selected and used three. The first two suggest enhanced human development outcomes with increased potential towards a more sustainable (SSP1[71]) or a less sustainable (SSP5[72]) economy. The third, SSP2[73], is a mid-way scenario, which assumes a future that mostly follows historical trends[70]. We selected these scenarios in combination with a low (SSP1-RCP2.6), intermediate (SSP2-RCP4.5), and high (SSP5-RCP8.5) greenhouse gas concentration scenario.

We apply a standard quantile-quantile (Q-Q) bias-correction[74,75] to the CMIP6 precipitation and temperature datasets for both of the historical simulations for the period 1901-2014, and all three future simulations for the period 2015-2100. Before the bias-correction, we first remap all simulated CMIP6 precipitation and temperature datasets to the same grid cell size ($0.5^\circ \times 0.5^\circ$) as the CRU-TS observation data. We then perform for each CMIP6 model, the Q-Q bias correction at each grid-point by mapping the quantile values (q_i) for the empirical cumulative distribution functions for each of the 12 months over the period 1901-2014 (for each grid point) onto the corresponding quantiles in the observational dataset (CRU-TS), so that the observed precipitation or temperature values associated with q_i become the bias-corrected value in the simulations. For the counterfactual (and future) simulations, we first determine, at each grid-point, for each value of precipitation or temperature (for each month) over the period 1901-2014 (2015-2100) the equivalent quantile (q_j) in the factual simulation and then identify the precipitation or temperature value associated with q_j in the observational dataset as the bias-corrected value. We detrended both precipitation and temperature datasets before applying the bias-correction procedure, and then added the trends back after[75].

For every climate dataset (all CRU-TS and CMIP6 models), we extract the average value of monthly precipitation and temperature within each ADM1 unit. To construct polynomial variables for temperature and precipitation (see below), all data were transformed at the grid cell level prior to aggregation to the ADM1 unit; extreme precipitation cutoffs were defined at the ADM1 level and so were applied after aggregation.

Statistical model

The influence of climatic conditions on malaria prevalence has been heavily studied using transmission models based in vector ecophysiology and calibrated using laboratory experiments[6,7]. The important benefit of this approach is that the mechanistic links

between a particular environmental condition (e.g., temperature) and malaria prevalence in the human population, such as effects on biting rate and survival probability, can be independently isolated. However, this approach is limited in its ability to generalize to real-world contexts, where complex socioeconomic factors interact with modeled relationships based on laboratory conditions. Clinical data, which measures malaria prevalence in human populations, has been used to validate modeled results[6], but inconsistent findings arise due to challenges in statistically isolating the role of climate from the many correlated factors influencing prevalence, such as public health interventions, drug resistance, conflict and social instability, and economic shocks[19,60,76,77,78].

This study seeks to provide generalizable population-scale evidence of the malaria-climate link across sub-Saharan Africa using field-collected clinical data and a statistical approach designed to isolate changing environmental conditions from spatiotemporal confounding factors. Specifically, we draw on the climate econometrics literature[47], which has developed causal inference approaches to quantify and project the impacts of anthropogenic climate change on a host of socioeconomic outcomes, from agricultural yields[79], to civil conflict[80], to all-cause mortality[48]. This approach is designed to approximate controlled experiments by semi-parametrically accounting for unobservable spatial and temporal confounding factors, isolating variation in the climate system that is as good as randomly assigned[81]. This approach is often referred to as "reduced-form", as it allows for a causal interpretation of recovered relationships between socioeconomic conditions and the climate, but it does not easily enable the researcher to isolate individual *mechanisms* linking a changing climate to shifts in outcomes (e.g., mosquito population dynamics or parasite development rates). However, causal estimates enable counterfactual simulation in which climate is changed and all other factors are held constant; this is the exercise conducted here and in many applications of climate econometric frameworks. Moreover, these relationships can be used to calibrate more structured transmission models by providing empirical grounding from observational data.

We develop a statistical model using monthly survey-based malaria prevalence data for children aged 2 to 10 ($Pf\text{PR}_{2-10}$) covering all of sub-Saharan Africa over 115 years. Our outcome variable is the average prevalence for each first administrative unit i (e.g., province or state) in country c during month m and year t, which we denote $Pf\text{PR}_{icmt}$. We estimate prevalence as a flexible function of monthly temperature T_{icmt} and precipitation P_{icmt} variables as follows:

$$\begin{aligned} Pf\text{PR}_{icmt} = f(T_{icmt}) + \sum_{\ell=0}^{L} g_\ell(P_{icm-\ell t}) + \alpha_i + \gamma_{rm} + h_c(\text{date}_{mt}) \\ + \delta_1 \mathbb{1}\{\text{intervention 1}\}_{mt} + \delta_2 \mathbb{1}\{\text{intervention 2}\}_{mt} + \varepsilon_{icmt} \end{aligned} \tag{1}$$

where $f(\cdot)$ and $g(\cdot)$ represent nonlinear transformations of grid-cell level temperature and precipitation conditions, respectively, and where ℓ subscripts indicate monthly temporal lags. In our main specification, we model $f(\cdot)$ as a quadratic in contemporaneous average temperature, while $g(\cdot)$ contains a vector of dummy variables indicating whether an

administrative unit's monthly rainfall can be categorized as drought (defined as $\leq 10\%$ of the long-run location- and month-specific mean) or flood (defined as $\geq 90\%$ of the long-run location- and month-specific mean) during month $m - \ell$. We allow for up to three monthly of lags (i.e., $L = 3$) for these extreme precipitation conditions in our main specification, based on hypotheses from prior literature regarding the timescales of larvae drying and of "flushing"[50,53,82]. A variety of sensitivity analyses detailed below demonstrate that key findings are robust to including lags for temperature (Figure S7), to the drought and flood cutoffs used for precipitation (Figures S8-S10), and to alternative functional forms of temperature (Figure S11).

Equation 1 uses a suite of semi-parametric spatiotemporal controls to isolate plausibly random variation in climatological conditions, following standard practices in the climate impacts literature.[47,45] First, α_i is a vector of indicator variables for each of 853 first administrative units (i.e., "ADM1" units) across our multi-country sample. These spatial "fixed effects" control for all time-invariant characteristics of an administrative unit that may confound the relationship between temperature, rainfall, and prevalence. For example, higher altitude regions may exhibit cooler temperatures, but they also may be composed of lower-income and more geographically isolated communities with limited access to malaria prevention interventions. By controlling for mean conditions in each location, these spatial fixed effects avoid conflating climate conditions with other geographic correlates.

Second, γ_{rm} is a vector of region-by-month-of-year indicator variables, where regions are defined using the Global Burden of Disease (GBD) regional definitions of western, southern, central, and eastern Africa (see Figure 2 in ref.[83]). These spatiotemporal fixed effects account for region-specific seasonality in prevalence that may spuriously relate to seasonally-varying climatological conditions. We allow these seasonal controls to vary by region because of large differences in climatological seasonality and in malaria cyclicality across sub-Saharan Africa[84], and we show below that our main findings are robust to more stringent seasonality controls defined at the country level (Figure S6). Third, $h_c(\cdot)$ is a nonlinear, country-specific function that controls for country-specific gradual trends that may confound the malaria-climate relationship, particularly under historical conditions of anthropogenic climate change. In our main specification, we model $h_c(\cdot)$ as a quadratic. Figure S6 shows that our results are robust to multiple alternative approaches to controlling for long-run trends that may vary across space.

Finally, the indicator variables $\mathbb{1}\{\text{intervention 1}\}_{mt}$ and $\mathbb{1}\{\text{intervention 2}\}_{mt}$ are equal to one when an observation falls into the 1955-1969 or 2000-2015 period, respectively. These two periods saw substantial malaria intervention programs across the subcontinent, leading to considerable declines in malaria that were unrelated to changes in the climate[4,85]. These indicator variables control for shocks to prevalence during these two periods, and the coefficients δ_1 and δ_2 allow for differential effectiveness of the two distinct intervention periods. While these variables are highly statistically significant (Table S2), our main findings are robust to their exclusion (Figure S6).

Together, these set of flexible controls imply that the residual variation in temperature and precipitation events used to identify the functions $f(\cdot)$ and $g(\cdot)$ is month-to-month

variation over time within the same location, after controlling for gradual country-specific trends, regional seasonality, and the aggregate effects of two substantial malaria prevention intervention programs. When reporting regression results directly (e.g., in Table S2), we cluster standard errors ε_{icmt} at the ADM1 level to account for serial correlation within the same location. When computing bootstrap samples (e.g., shown in Figure 2), we repeatedly re-estimate Equation 1 after block-resampling the full dataset using ADM1-level blocks to account for this same serial correlation.

Statistical model sensitivity and robustness

In this section, we describe a set of model sensitivity analyses that probe the robustness of our empirical model. Specifically, we investigate sensitivity of our key findings to: alternative spatiotemporal controls; inclusion of dynamic temperature effects; alternative definitions of extreme rainfall events; and alternative functional forms for the prevalence-temperature relationship.

Alternative spatiotemporal controls

Our preferred empirical specification in Equation 1 includes first administrative unit fixed effects (i.e., indicator variables), region-by-month-of-year fixed effects, country-specific quadratic time trends, and two indicator variables for each of two malaria intervention periods (1955-1969 and 2000-2015). Figure S6 shows that our estimated prevalence-temperature relationship is highly robust to many alternative spatial and temporal controls. All panels in this figure include ADM1 fixed effects to control for time-invariant characteristics that may confound the relationship between prevalence and temperature, but each panel varies in the additional spatial and/or temporal controls included in the regression. A tabular version of these results is shown in Table S2. While the temperature at which prevalence peaks changes slightly across model specifications, it remains within a degree of the 24.9°C value from our preferred specification for most models, particularly those including time trends that are spatially differentiated (note that peak temperatures indicated in Figure S6 are rounded to the nearest degree for display purposes). Predictably, stringent controls, such as region-by-year and country-by-month fixed effects, tend to increase statistical uncertainty. However, overall the estimated shape and magnitude of the prevalence-temperature relationship remain robust to alternative spatial and temporal controls.

Dynamic temperature effects

Our preferred empirical specification estimates contemporaneous (within one month) and lagged (up to three months) effects of extreme rainfall on malaria prevalence, but only contemporaneous effects of temperature. While it is possible that temperature also exhibits lagged effects, we show in Figure S7 that the cumulative effect of temperature on $Pf\mathrm{PR}_{2-10}$ is very similar whether zero, one, two, or three months of lagged temperatures are accounted for. The prevalence response to temperature does become slightly stronger

with three months of lags, suggesting that our historical and future climate predictions shown throughout the main text may be somewhat conservative. However, overall these findings suggest that climate change impact predictions are unlikely to change meaningfully under different assumptions of the lag structure of temperature exposure.

Alternative definitions of extreme rainfall events

Our main empirical specification defines drought as months for which total precipitation is less than or equal to 10% of the long-run location- and month-specific mean. Flood is analogously defined as months for which total precipitation is greater than or equal to 90% of the long-run location- and month-specific mean. Here, we investigate the sensitivity of our main findings to these definitions. To do so, we systematically vary both the drought and flood cutoff values, ranging from <1% to <20% for drought and from >85% to >95% for flood. Figure S8 shows that the relationship between malaria prevalence and temperature is insensitive to the definition of drought and flood events. Figure S9 shows that under most drought and flood definitions, extremely low precipitation events have a negative effect on prevalence with a lag of 1-2 months. However, this effect is rarely statistically significant. Figure S10 shows that extremely high rainfall events increase prevalence with a lag of 2-3 months, a result that is statistically significant and highly robust to alternative drought and flood definitions. In general, these sensitivity analyses show that our main findings are not sensitive to the specific definitions of drought and flood used in estimation of Equation 1.

Alternative functional forms for the prevalence-temperature relationship

Following from theoretical and laboratory-based literature (e.g., refs.[6,7]), we model the prevalence-temperature relationship as quadratic. However, Figure S11 shows that this relationship is similar when more flexible functional forms are used. In particular, the temperature at which prevalence peaks changes little when higher order polynomials are estimated. Estimating higher order polynomials increases uncertainty, particularly in the tails of the temperature distribution, but point estimates are similar across the majority of the observed temperature range.

Predictions

In both historical and future simulations, we apply the estimated panel regression to calculate the effect of climate change on $Pf\mathrm{PR}_{2-10}$. Our predictions capture the full range of statistical uncertainty (1,000 bootstrapped model estimates) and climate model uncertainty (10 climate models), producing a total of 10,000 estimates of historical or future impacts in any given scenario. Each of these 10,000 estimates is normalized to a long-run baseline (past: 1901-1930; present: 2015-2020) before estimates are averaged, creating an estimate of climate change impacts relative to that baseline. In our historical analyses, we only use these models to estimate changes in prevalence attributable to climate change: while the panel regression model accounts for other historical drivers

through the fixed effects structure, these are not the focus of our analysis, and so we choose not to estimate total prevalence including these effects. Similarly, we elect not to make assumptions about non-climate drivers of malaria prevalence in the future, and thus do not apply the model to predict future trends in overall prevalence.

For overall trends (e.g., reported in Figures 2D, 3D, and 4D), we generated continent-wide averages or four regional averages using the unweighted average of estimates for each ADM1 unit. This is a deliberate oversimplification, as we do not adjust averages based on either ADM1 units' land area or the estimated population they contain; we made this decision based on the challenges of reconstructing historical population density at fine scales, as well as the need to otherwise make assumptions about how disease burden is allocated over space (e.g., the distribution of transmission across rural or urban areas). For similar reasons, we chose not to estimate the effect of prevalence changes on overall malaria incidence. Although some studies have attempted this using a linear conversion with total population[86], proper estimation of incidence (and the effects of treatment variables, through prevalence, on case burden) requires malaria transmission models that require substantially more demographic assumptions[85]. Future work could explore both of these methodologically-complex directions, and potentially generate finer-scale estimates of how many cases of childhood malaria, and resulting deaths, are attributable to climate change.

Acknowledgements

We thank Sadie Ryan and Rory Gibb for thoughtful conversations that supported this work, and Jonathan Proctor for constructive feedback on the manuscript. CHT was supported by the University of Cape Town Future Leaders Programme and by the FLAIR Fellowship Programme: a partnership between the African Academy of Sciences and the Royal Society funded by the UK Government's Global Challenges Research Fund. RCO was supported by the Carnegie Corporation of New York through the Development of Emerging Academic Leaders (DEAL) in Africa and the German Academic Exchange Service (DAAD) ClimapAfrica programme.

Data Availability

No original data are generated or reported in our study. All data used in analyses, including both malaria and climate data, is freely available and referenced in the Methods.

Code Availability

All code is available at github.com/cjcarlson/falciparum.

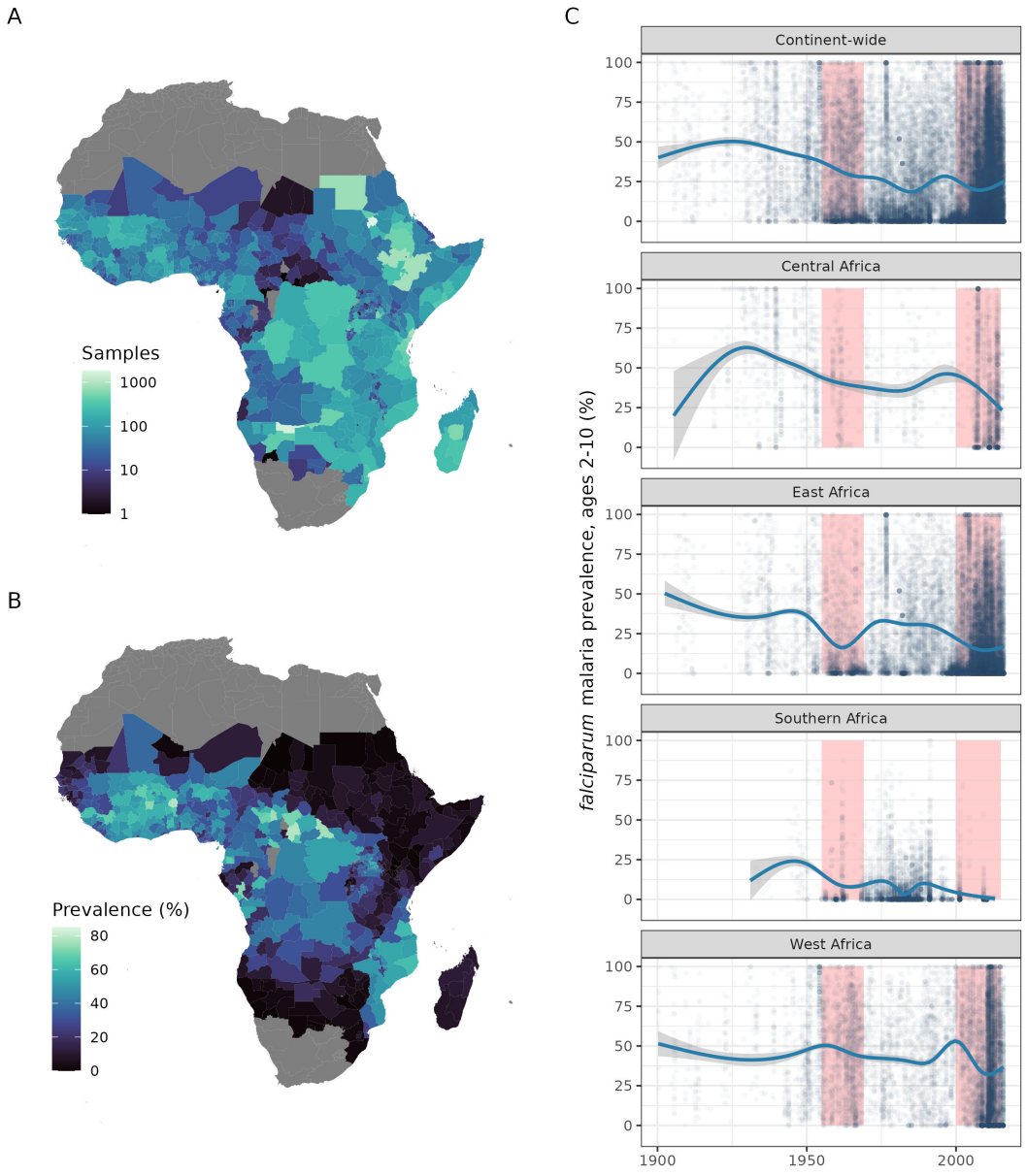

Figure 1: **Malaria prevalence observations from 1900 to 2015.** (A) The total number of malaria prevalence surveys in children ages 2 to 10 in the 20^{th} and early 21^{st} century, as measured by Snow *et al.*[4] and aggregated to the first administrative unit (ADM1). (B) Mean reported prevalence of childhood malaria over the entire sample (1900-2015, with temporal coverage varying across space). (C) Observed trends in malaria prevalence, broken down by Global Burden of Disease Study regions (see main text): each point is a single survey in the original dataset, while generalized additive models are used to construct estimated trend lines (shown in solid blue, with grey shading showing the model's 95% confidence interval). Pink vertical bars indicate notable periods of successful malaria prevention intervention: the Global Malaria Eradication Programme (1955-1969) and the modern period including the Roll Back Malaria programs and Global Technical Strategy (2000-2014).

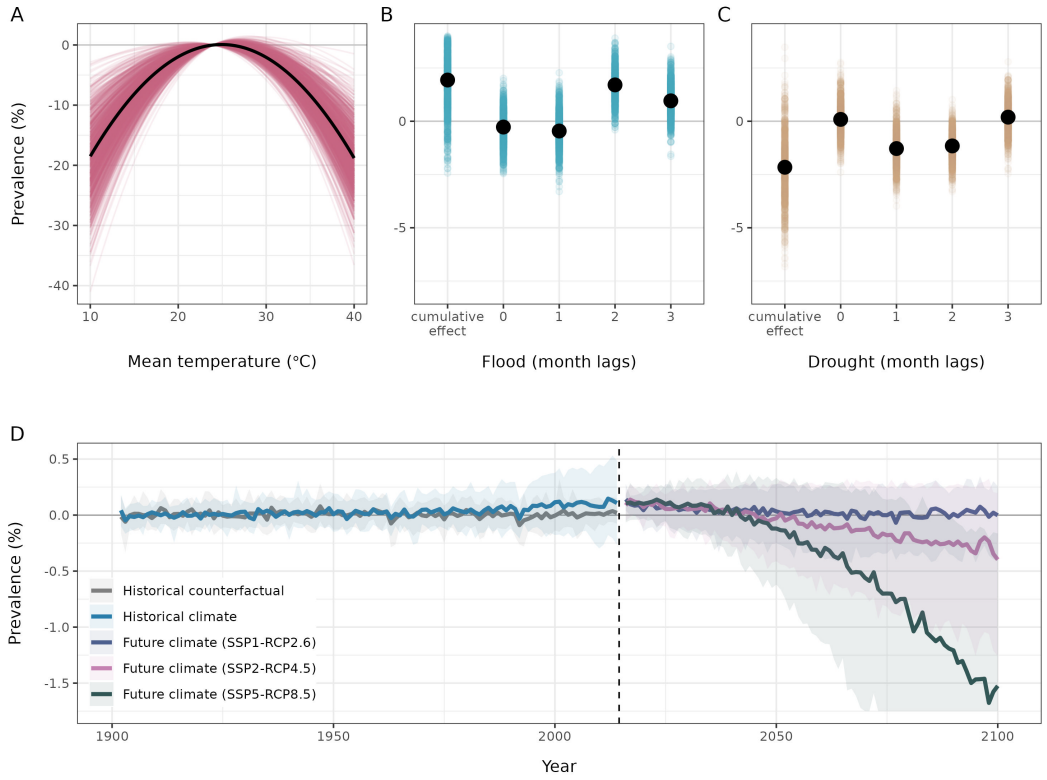

Figure 2: **Empirical estimates of prevalence-climate relationships and predictions of climate change impacts from 1901 to 2100.** (A) The estimated relationship between temperature and prevalence (point estimate in black; bootstrapped estimates in red). (B,C) The effects of extreme precipitation events (flood and drought) in the month they occur (0 lag) and after time has passed (1, 2, 3 month lags), as well as the cumulative impact across the first three months; point estimates from the main model (black) are accompanied by bootstrap estimates (blue, brown). (D) Predicted change in prevalence attributable to anthropogenic climate change in the recent past (real historical climate given in blue; counterfactual without anthropogenic warming in grey) and in the future for low (blue: SSP1-RCP2.6), intermediate (pink: SSP2-RCP4.5), and high (green: SSP5-RCP8.5) emissions scenarios. Thick lines are the median estimates across all 10,000 simulations; shading indicates the 5^{th} and 95^{th} percentiles of this distribution, and is truncated at the lower axis limits for visualization purposes only (the full interval is shown in Figure S5A). Historical estimates are shown relative to an average baseline across 1901 to 1930. Future estimates are shown relative to a baseline across 2015 to 2019, added to the end-of-historical baseline (2010 to 2014). Years with incomplete predictions due to lag effects (1901 and 2015) are not displayed.

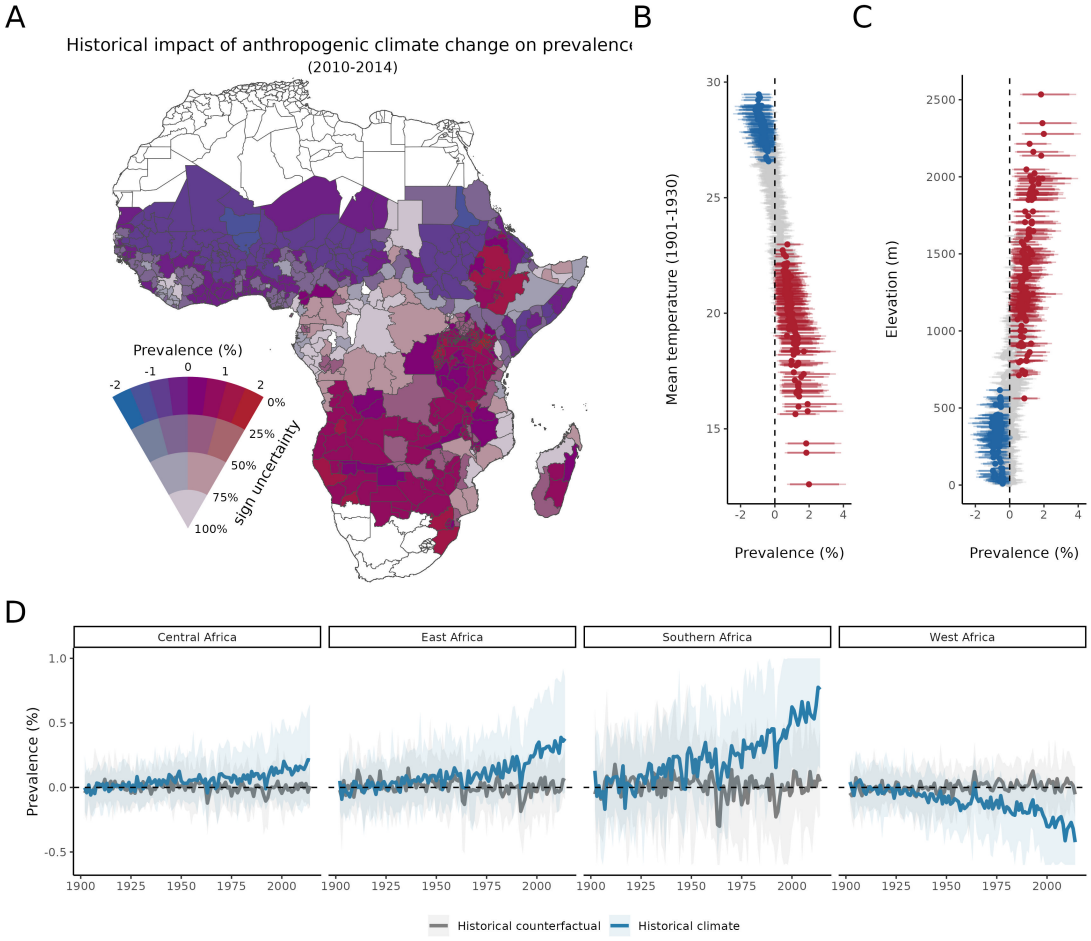

Figure 3: **Historical changes in malaria prevalence attributable to anthropogenic climate change from 1901 to 2014.** (A) Estimated change in prevalence attributable to anthropogenic climate change in each administrative unit, based on the difference between the historical climate in 2010-2014 and a counterfactual scenario for the same period simulated without anthropogenic warming. Sign uncertainty is the percentage of the 10,000 simulations that estimate an increase (for positive point estimates) or decrease (for negative point estimates) in prevalence due to anthropogenic climate change. An uncertainty of 0% implies that all models predict a positive or negative trend, while an uncertainty close to 100% indicates a near-even split of simulations showing an increase or decrease in prevalence. (B) Estimated change in prevalence attributable to anthropogenic climate change (difference between factual and counterfactual scenario in 2010-2014) in each administrative polygon, compared to the baseline mean temperature at the start of the 20^{th} century (averaged over 1901-1930); error bars indicate both 90% (thicker lines) and 95% (thinner lines) confidence intervals. Points and lines are colored based on the 90% confidence interval: blue for negative effects, red for positive effects, and grey for non-significant effects. (C) Estimated change in prevalence attributable to anthropogenic climate change in each administrative polygon, compared to average elevation; error bars indicate both 90% and 95% confidence intervals, colored as in (B). (D) Predicted historical changes in prevalence by year, broken down by region. As in Figure 2, predictions based on true historical climate (blue) are compared to counterfactual predictions without anthropogenic warming (grey), relative to a 1901 to 1930 baseline. Thick lines are the median estimate across all 10,000 simulations; for visualization purposes, shading indicates the 90% confidence interval, and is truncated at the upper and lower axis limits. Plots begin in 1902 with the first full year of predictions (due to lag effects).

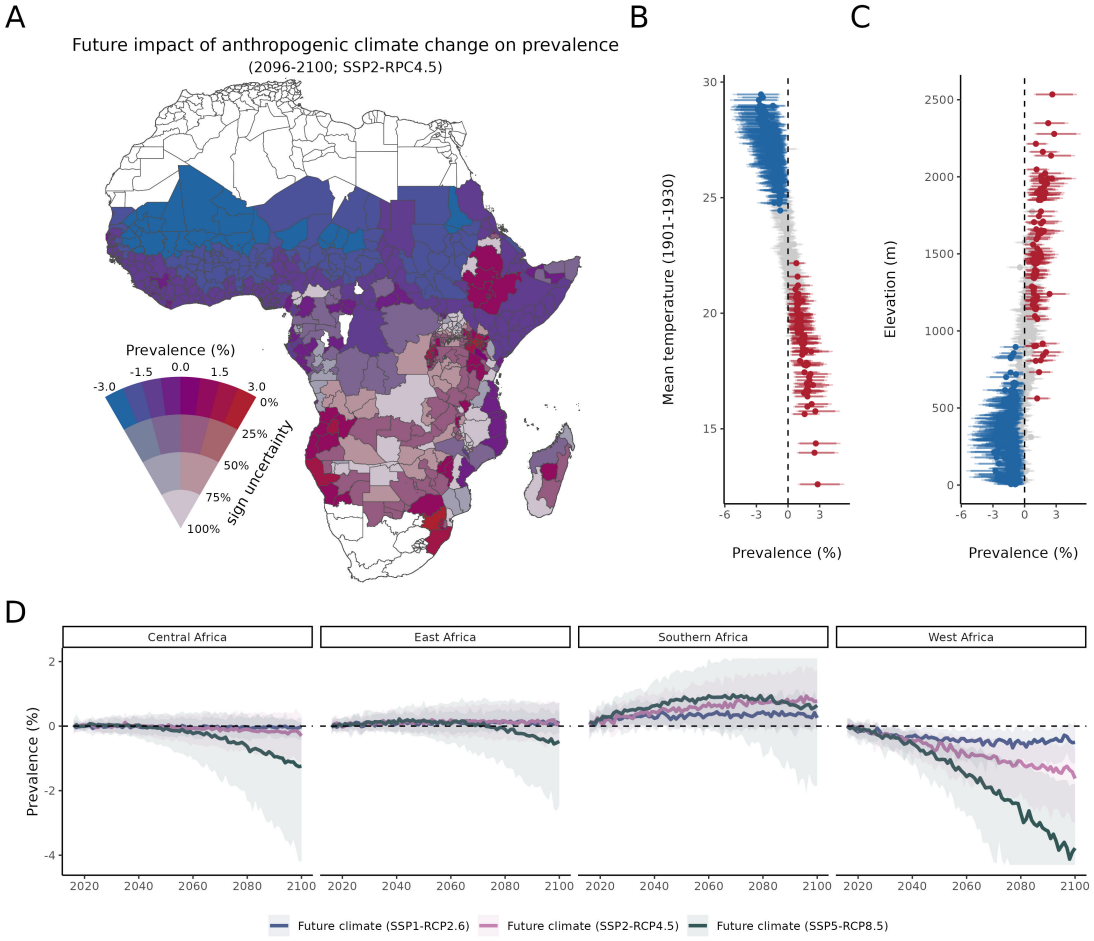

Figure 4: **Projected future changes in malaria prevalence driven by climate change from 2015 to 2100.** (A) Projected climate-driven changes in prevalence by the end of the century (2096-2100), compared to the present day (2015-2020), for an intermediate emissions scenario (SSP2-RCP4.5). Sign uncertainty is the percentage of the 10,000 simulations that estimate an increase (for positive point estimates) or decrease (for negative point estimates) in prevalence due to future climate change. An uncertainty of 0% implies that all models predict a positive or negative trend, while an uncertainty close to 100% indicates a near-even split of simulations showing an increase or decrease in prevalence. (B) Projected change in prevalence due to climate change by the end of the century (2096-2100) in each administrative polygon, estimated for SSP2-RCP4.5, compared to the baseline mean temperature at the start of the 20^{th} century; error bars indicate both 90% (thicker lines) and 95% (thinner lines) confidence intervals. Points and lines are colored based on the 90% confidence interval: blue for negative effects, red for positive effects, and grey for non-significant effects. (C) Projected change in prevalence due to climate change by the end of the century (2096-2100) in each administrative polygon, estimated for SSP2-RCP4.5, compared to average elevation; error bars indicate both 90% and 95% confidence intervals, colored as in (B). (D) Projected changes in prevalence by year across all scenarios by region. Projections are given relative to the mean from 2015-2019, and as in Figure 2, and line color indicates scenario (blue: SSP1-RCP2.6; pink: SSP2-RCP4.5; green: SSP5-RCP8.5). Thick lines are the median estimate across all 10,000 simulations; for visualization purposes, shading indicates the 90% confidence interval, and is truncated at the upper and lower axis limits. Plots begin in 2016 with the first full year of predictions (due to lag effects).

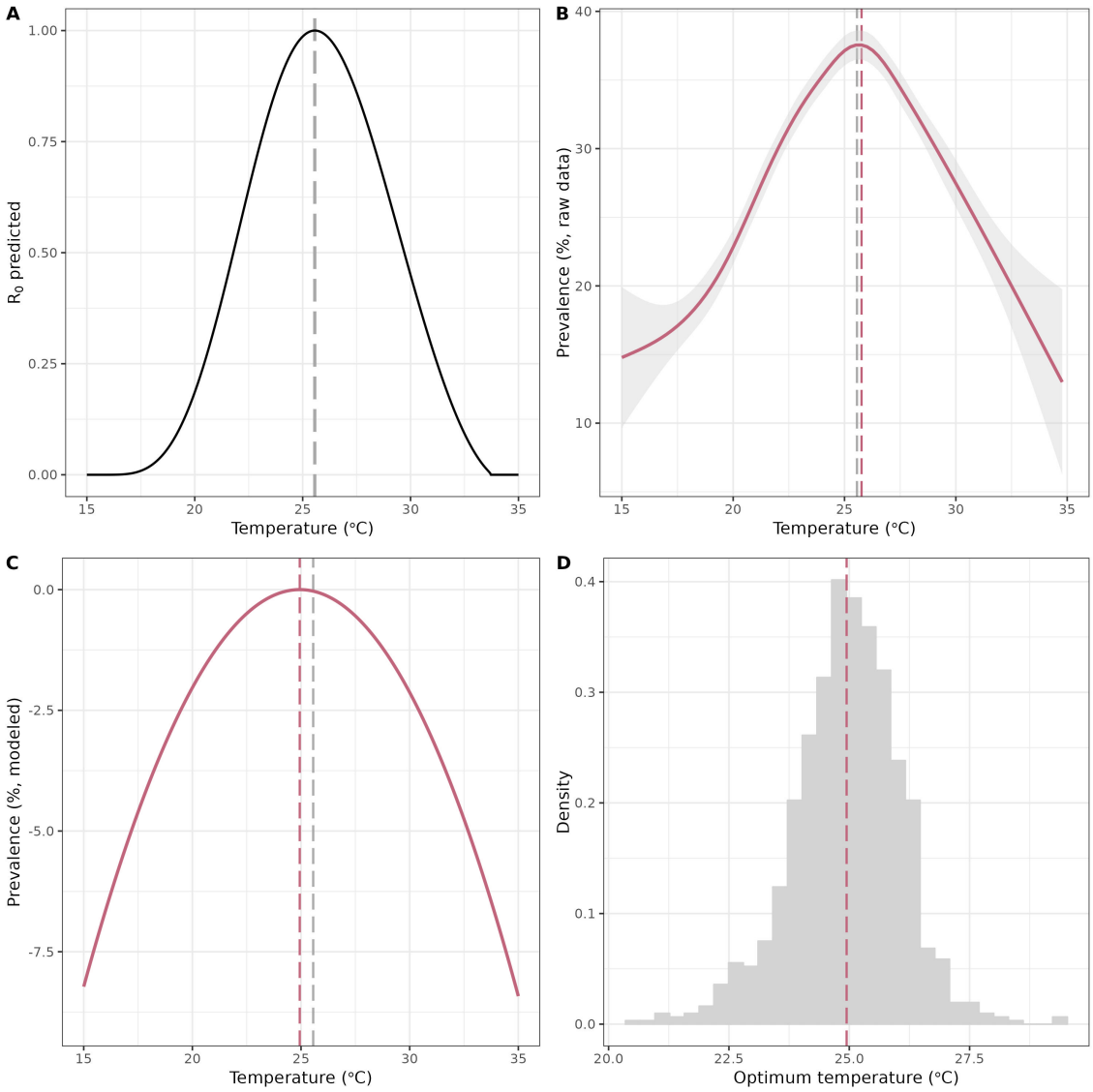

Figure S1: **Malaria prevalence follows biological expectations.** (A) The theoretical expectation for $R_0(T)$, the scaled partial response of the basic reproduction number to temperature, estimated based on laboratory experiments (black line)[6]. Transmission peaks around an estimated optimum of 25.6 °C (grey dashed line). (B) Observed malaria prevalence data from Snow *et al.*[4] matched to monthly temperature from CRU weather station data, summarized and smoothed using a generalized additive model. The observed optimum temperature (red dashed line) closely matches expectations based on laboratory experiments (grey dashed line). (C) Main panel regression estimate for prevalence response to temperature (also shown in Figure 2A). The modeled optimum temperature (red dashed line) is slightly lower than in laboratory experiments (grey dashed line). (D) Histogram of optimum temperatures derived from 1,000 bootstrapped estimates of the panel regression model shown in panel (C). The mean optimum temperature across all bootstrap samples (red dashed line) is identical to the optimum shown in panel C.

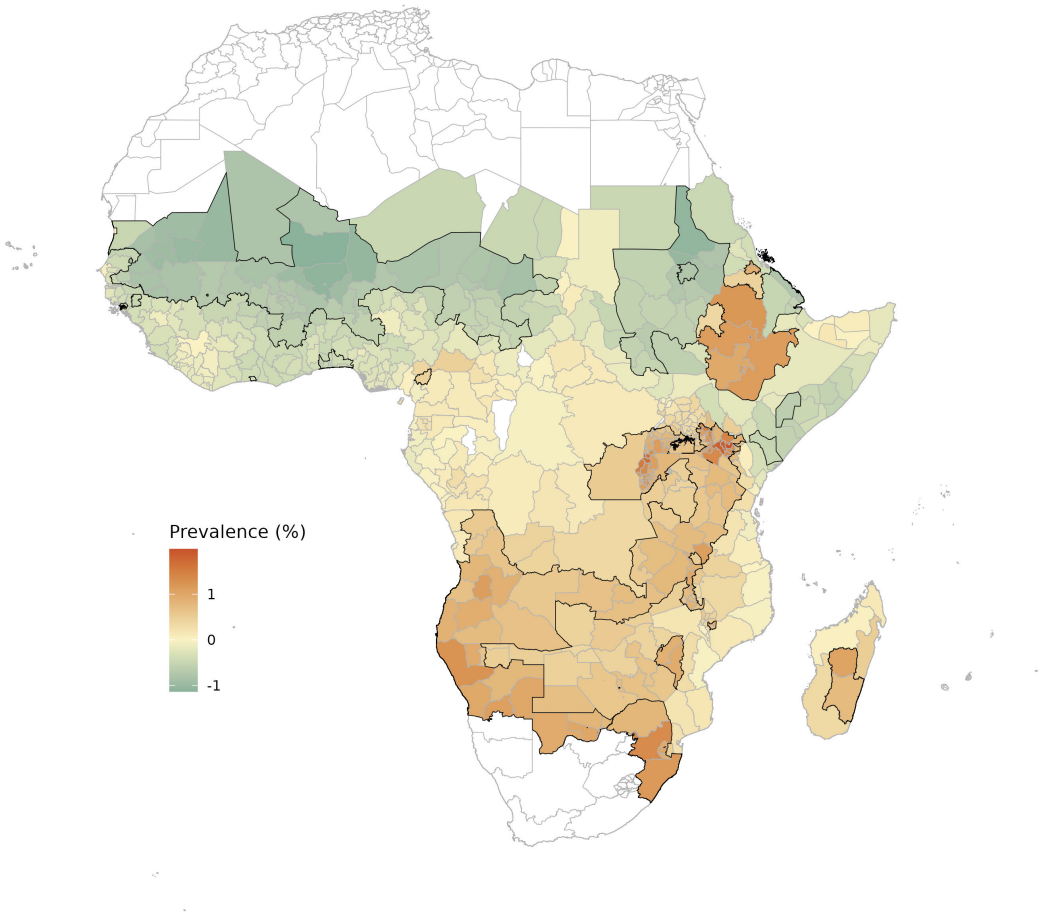

Figure S2: **Historical changes in malaria prevalence attributable to anthropogenic climate change from 1901 to 2014.** Map shows the estimated change in prevalence attributable to anthropogenic climate change in each administrative unit, based on the difference between the historical climate in 2010-2014 and a counterfactual scenario for the same period simulated without anthropogenic warming. Polygons with a black solid outline indicate areas with changes that were statistically significant ($\alpha = 0.05$) based on the sign of 10,000 bootstrapped simulations. Mean estimates shown here provide the same information as in Figure 3, but on a single color scale (*i.e.*, no uncertainty visualization).

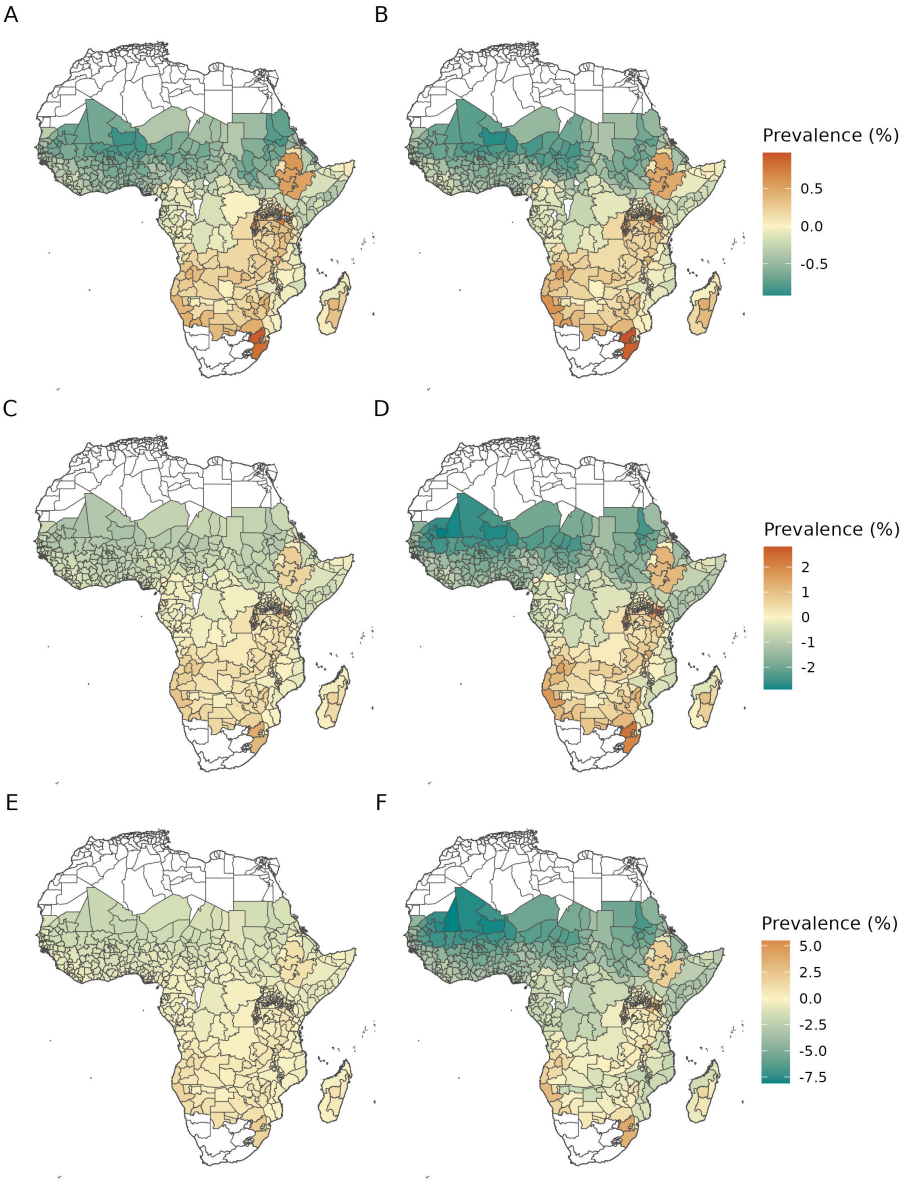

Figure S3: **Projected future changes in malaria prevalence driven by climate change from 2015 to 2100.** Maps show the estimated change in prevalence due to anthropogenic climate change (in percentage points) in low-emissions (SSP1-RCP2.6; A,B), moderate-emissions (SSP2-RCP4.5; C,D), and high-emissions (SSP5-RCP8.5; E,F) scenarios, projected to mid-century (2048-2052; A,C,E) or the end of the century (2096-2100; B,D,F). Projections are reported as differences relative to a present-day baseline (2015-2019). Mean estimates in panel D provide the same information as in Figure 4, but on a single color scale (*i.e.*, no uncertainty visualization).

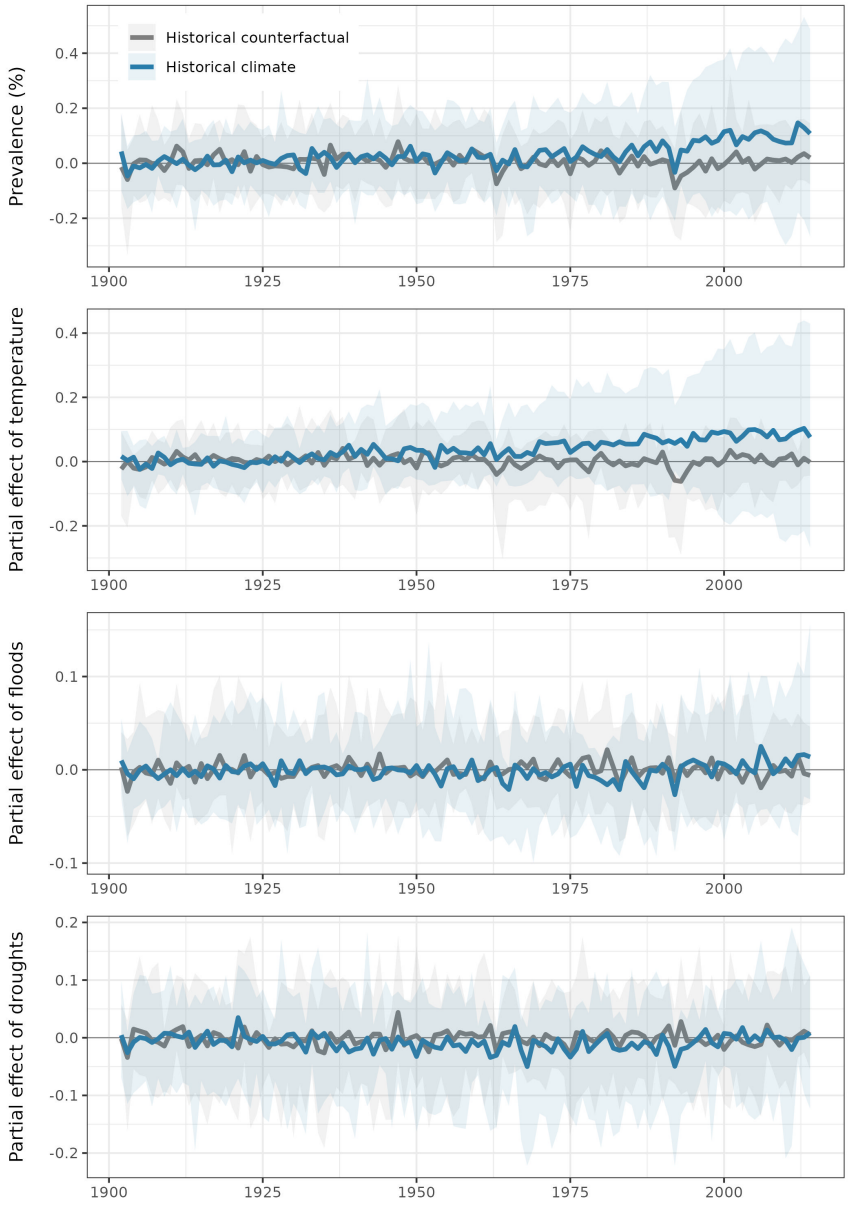

Figure S4: **Historical impacts of climate change decomposed by variable.** Partial predictions of changes in malaria attributable to anthropogenic climate change are made based on all climate variables (top row), temperature (second row), flood shocks (third row), and drought shocks (fourth row). As in Figure 2, predictions based on true historical climate (blue) are compared to counterfactual predictions without anthropogenic warming (grey), relative to a 1901 to 1930 baseline. Thick lines are the median estimate across all 10,000 simulations; shading indicates the 5^{th} and 95^{th} percentiles. Plots begin in 1902 with the first full year of predictions (due to lag effects).

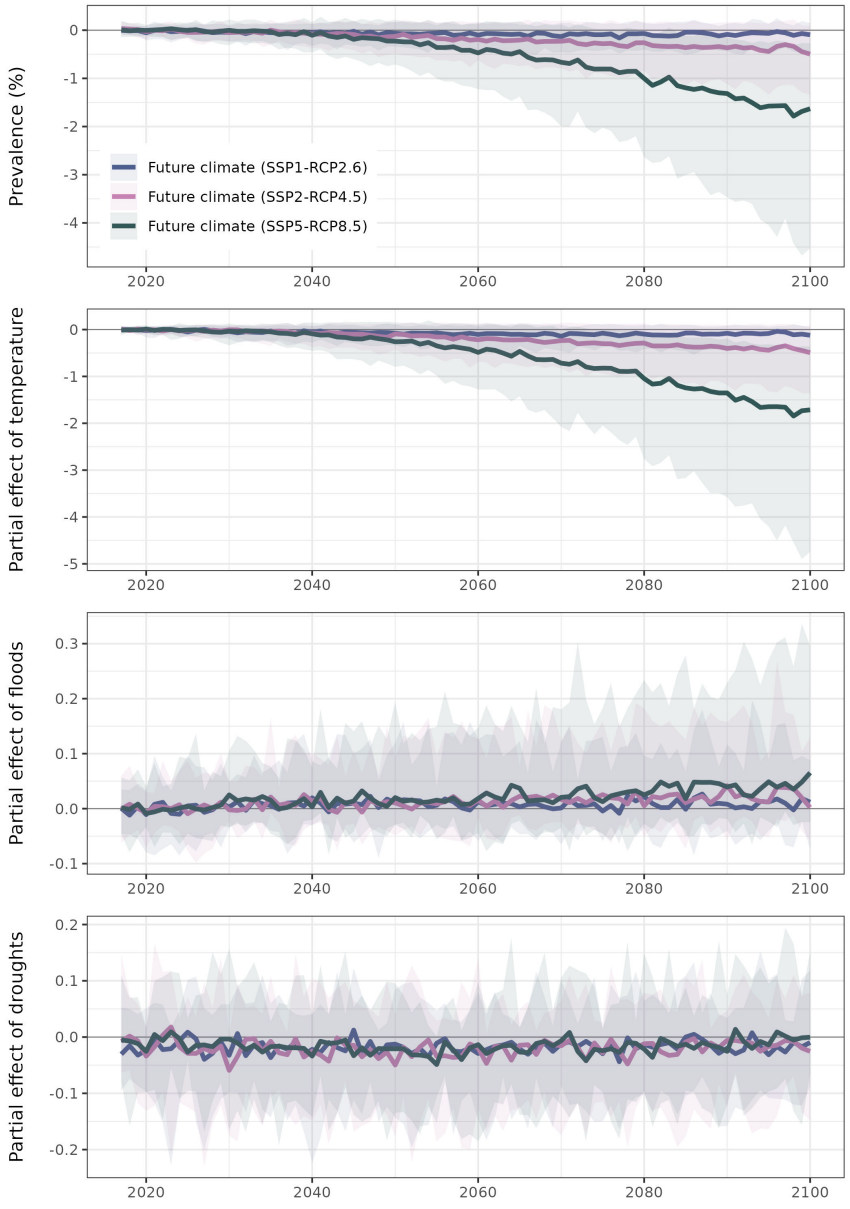

Figure S5: **Future impacts of climate change decomposed by variable.** Partial predictions of changes in malaria attributable to future climate change are made based on all climate variables (top row) temperature (second row), flood shocks (third row), and drought shocks (fourth row). Projections are shown relative to the mean prevalence from 2015-2020, and as in Figure 2, line color indicates emissions scenario (blue: SSP1-RCP2.6; pink: SSP2-RCP4.5; green: SSP5-RCP8.5). Thick lines are the median estimate across all 10,000 simulations; shading indicates the 5^{th} and 95^{th} percentiles. Plots begin in 2016 with the first full year of predictions (due to lag effects).

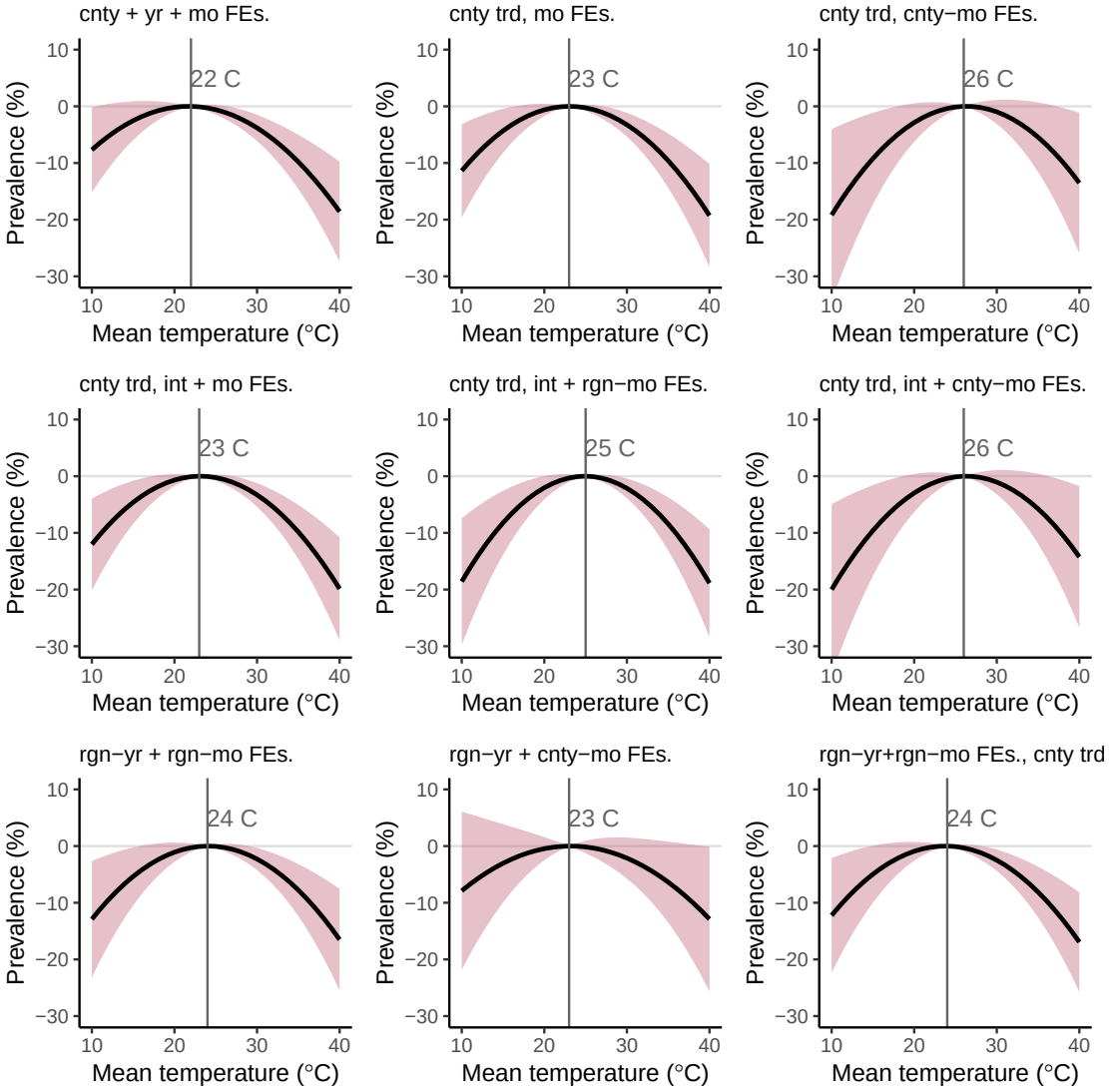

Figure S6: **Sensitivity of the $Pf\mathbf{PR}_{2-10}$-temperature relationship to alternative spatiotemporal controls.** All panels show the estimated relationship between malaria prevalence for children aged 2-10 and monthly average temperature and all include fixed effects (i.e., dummy variables) at the scale of the first administrative unit (i.e., ADM1). All temperature responses are plotted relative to the model-specific temperature at which prevalence is maximized; this peak temperature is indicated in grey text and with a vertical grey line in each panel. From top-left to bottom-right, model controls are: country, year, and month fixed effects; country-specific quadratic time trends and month fixed effects; country-specific quadratic time trends and country-by-month fixed effects; country-specific quadratic time trends and intervention period and month fixed effects; country-specific quadratic time trends and intervention period and region-by-month fixed effects; country-specific quadratic time trends and intervention period and country-by-month fixed effects; region-by-year and region-by-month fixed effects; region-by-year and country-by-month fixed effects; and region-by-year and region-by-month fixed effects and country-specific linear time trends. The preferred specification used throughout the main text is the center panel, which includes country-specific quadratic time trends and intervention period and region-by-month fixed effects. In all panels, "region" refers to the Global Burden of Disease regional definitions of western, southern, central, and eastern Africa. All standard errors are clustered at the first administrative unit (e.g., province) level.

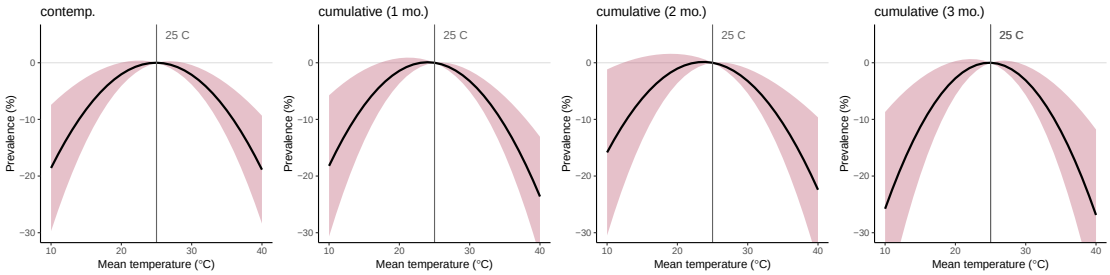

Figure S7: **Cumulative effect of contemporaneous and lagged temperature on $Pf\mathbf{PR}_{2-10}$.** All panels show the estimated relationship between malaria prevalence for children aged 2-10 and monthly average temperature and are plotted relative to a monthly average temperature of 25°C. The first panel shows the effect of monthly average temperature on the same month's average prevalence (this is the main estimate used throughout the main text). The second panel shows the cumulative effect of contemporaneous temperature and the prior month's temperature on prevalence, while the last two columns show analogous results for two and three months of lags, respectively. In all specifications, three months of lagged precipitation extremes are included, as well as all other controls shown in Equation 1. All standard errors are clustered at the first administrative unit (e.g., province) level.

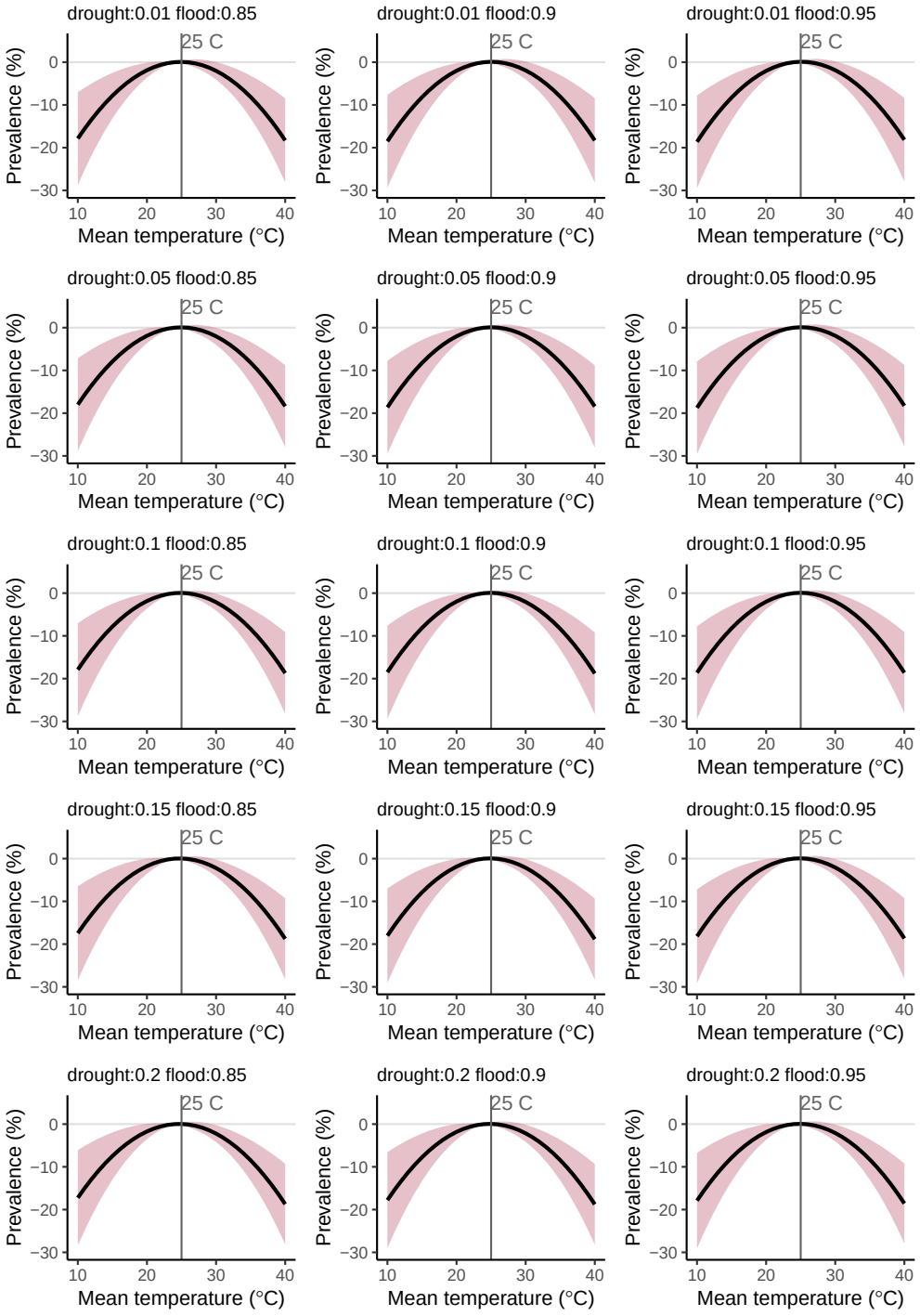

Figure S8: **Sensitivity of $Pf\mathbf{PR}_{2-10}$-temperature relationship to alternative drought and flood definitions.** All panels show the estimated relationship between malaria prevalence for children aged 2-10 and monthly average temperature and are plotted relative to a monthly average temperature of 25°C. Cutoff values for drought and flood definitions are given in the titles of each panel. For example, the first panel in the upper left defines drought as monthly total precipitation that falls below 1% of the long-run location- and month-specific mean, and defines flood as monthly total precipitation that falls above 85% of the long-run location- and month-specific mean. In all specifications, three months of lagged precipitation extremes are included, as well as all other controls shown in Equation 1. The main specification used throughout the paper uses a drought cutoff of 10% and a flood cutoff of 90%. All standard errors are clustered at the first administrative unit (e.g., province) level.

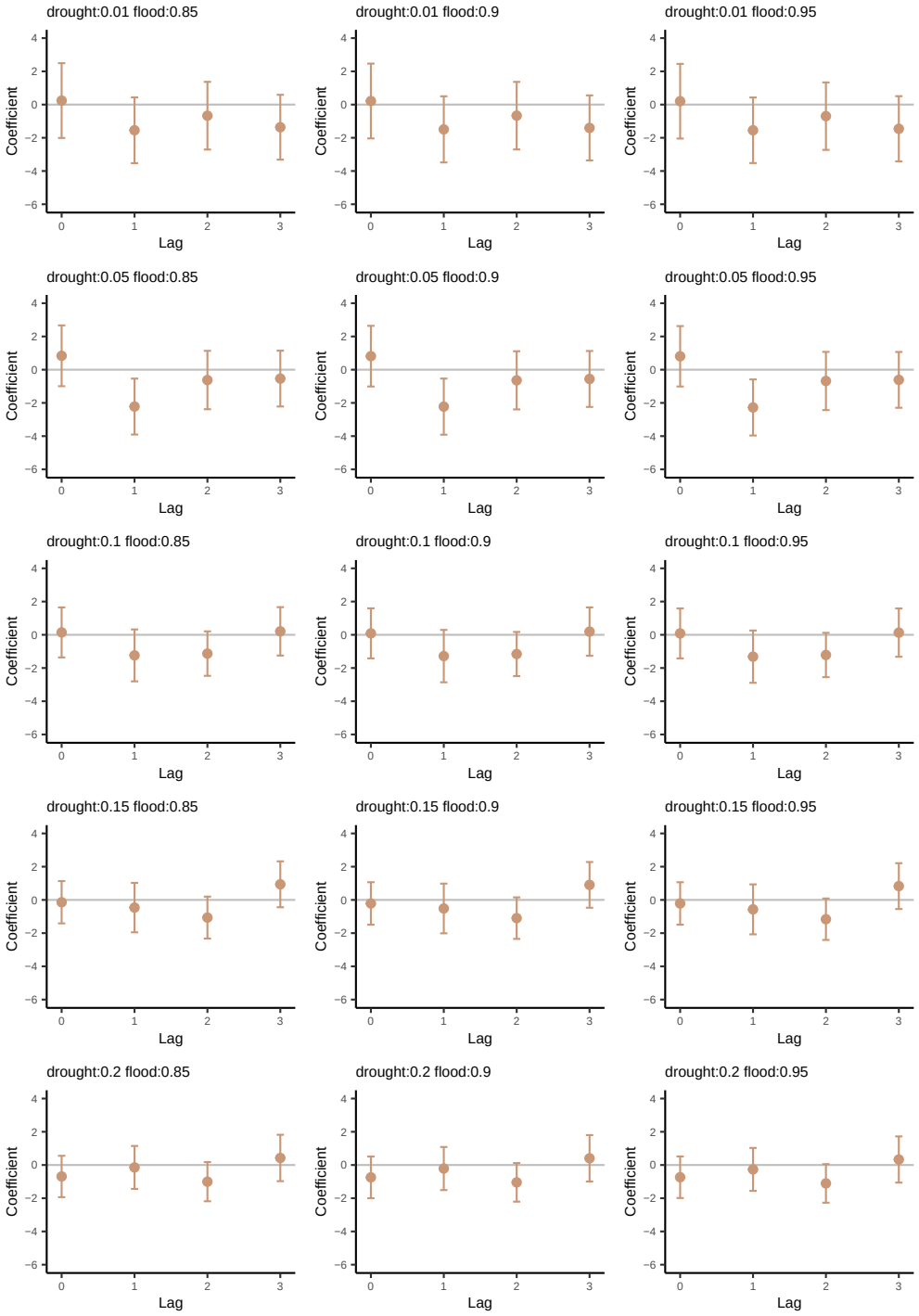

Figure S9: **Sensitivity of $Pf\mathbf{PR}_{2-10}$-drought relationship to alternative drought and flood definitions.** All panels show the estimated relationship between malaria prevalence for children aged 2-10 and contemporaneous and lagged drought events. Point estimates are given by solid circles, while vertical bars indicate 95% confidence intervals. Cutoff values for drought and flood definitions are given in the titles of each panel. For example, the first panel in the upper left defines drought as monthly total precipitation that falls below 1% of the long-run location- and month-specific mean, and defines flood as monthly total precipitation that falls above 85% of the long-run location- and month-specific mean. In all specifications, three months of lagged precipitation extremes are included, as well as all other controls shown in Equation 1. The main specification used throughout the paper uses a drought cutoff of 10% and a flood cutoff of 90%. All standard errors are clustered at the first administrative unit (e.g., province) level.

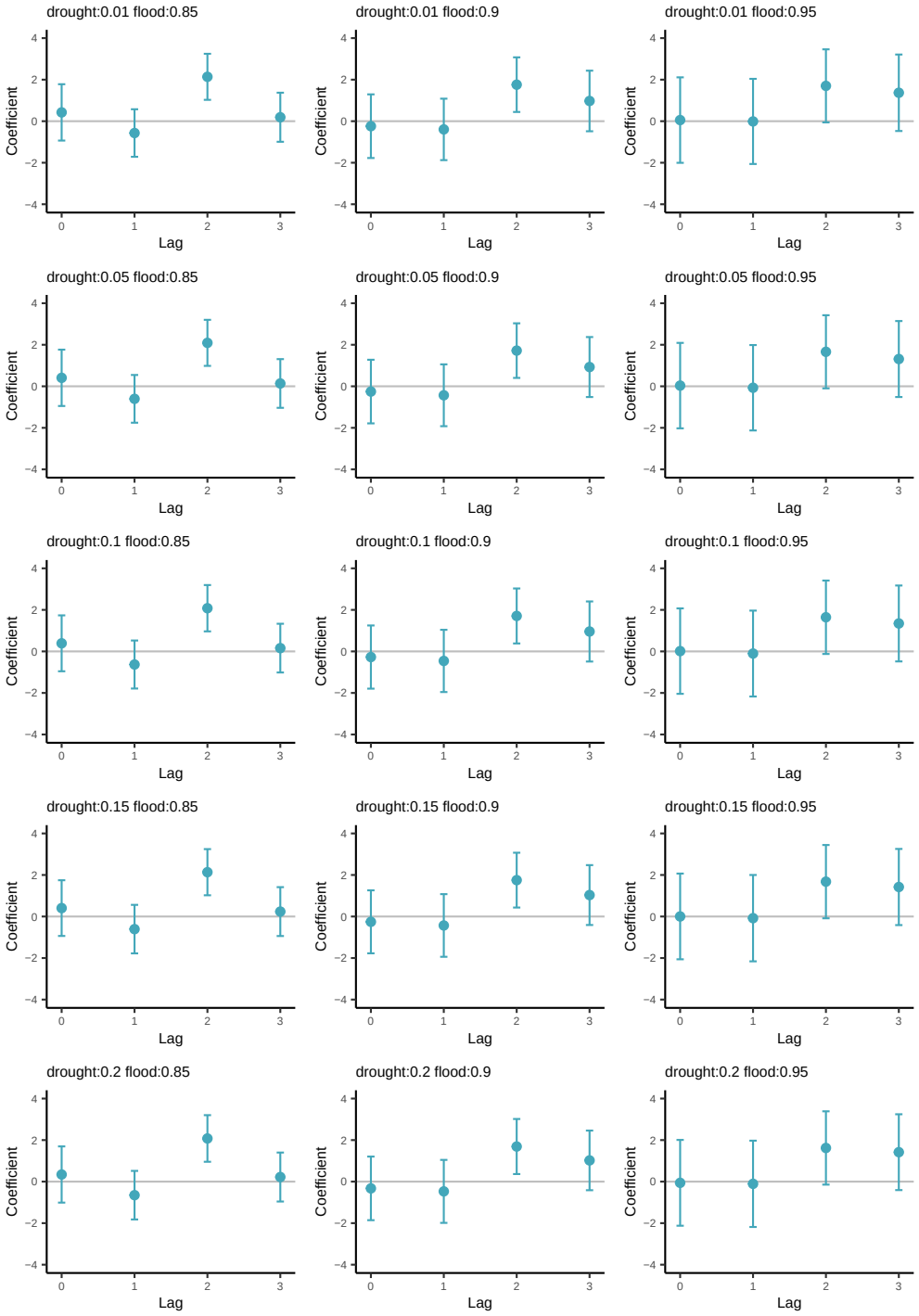

Figure S10: **Sensitivity of $Pf\mathbf{PR}_{2-10}$-flood relationship to alternative drought and flood definitions.** All panels show the estimated relationship between malaria prevalence for children aged 2-10 and contemporaneous and lagged flood events. Point estimates are given by solid circles, while vertical bars indicate 95% confidence intervals. Cutoff values for drought and flood definitions are given in the titles of each panel. For example, the first panel in the upper left defines drought as monthly total precipitation that falls below 1% of the long-run location- and month-specific mean, and defines flood as monthly total precipitation that falls above 85% of the long-run location- and month-specific mean. In all specifications, three months of lagged precipitation extremes are included, as well as all other controls shown in Equation 1. The main specification used throughout the paper uses a drought cutoff of 10% and a flood cutoff of 90%. All standard errors are clustered at the first administrative unit (e.g., province) level.

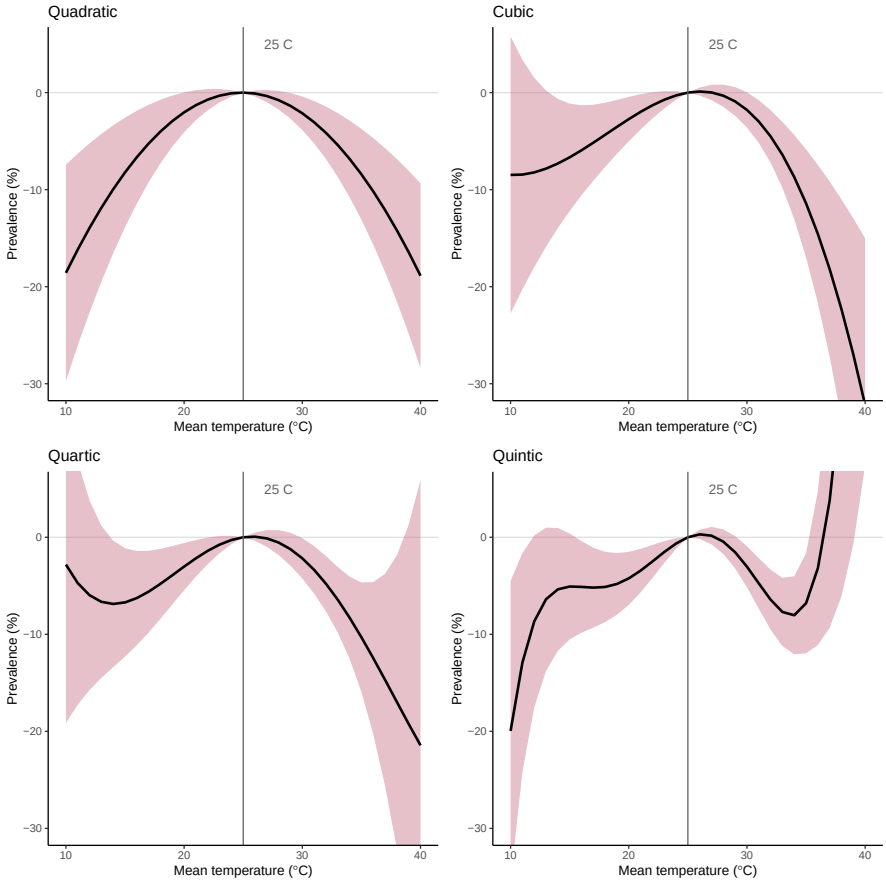

Figure S11: **Alternative functional forms for the $Pf\mathbf{PR}_{2-10}$-temperature relationship.** All panels show the estimated relationship between malaria prevalence for children aged 2-10 and monthly average temperature and are plotted relative to a monthly average temperature of 25°C. Starting in the upper left, the first panel shows the paper's main specification, a quadratic functional form for the prevalence-temperature relationship. The second panel shows a cubic functional form, the third a quartic, and the fourth a quintic. All standard errors are clustered at the first administrative unit (e.g., province) level.

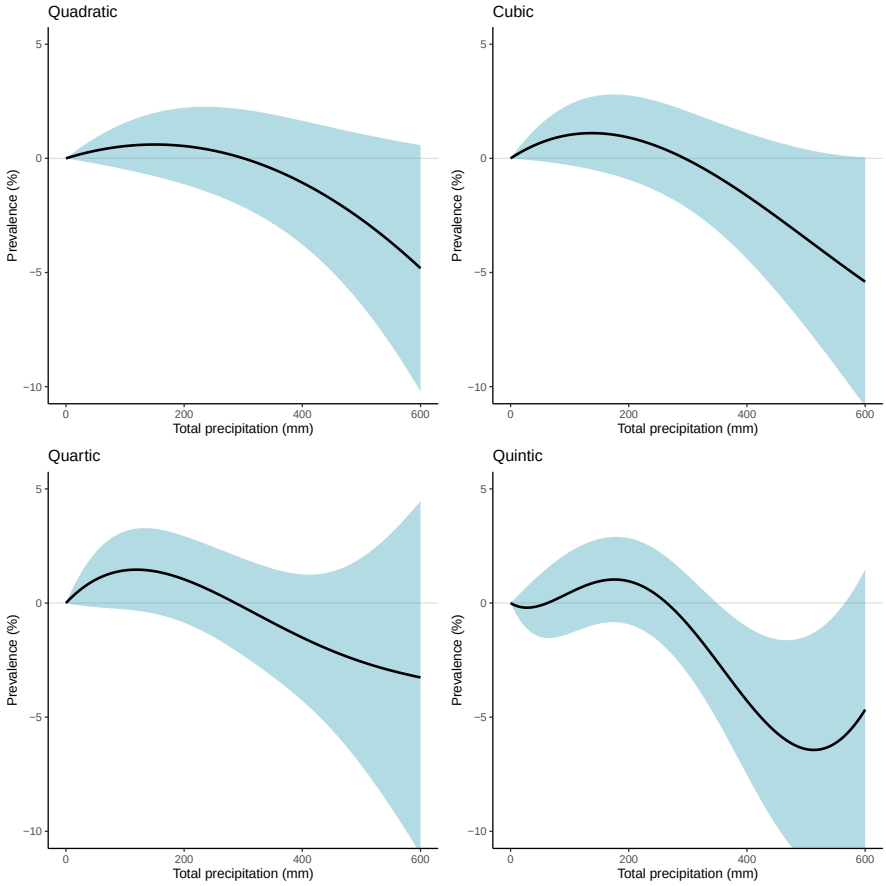

Figure S12: **Non-linearities in the $Pf\mathbf{PR}_{2-10}$-precipitation relationship.** All panels show the estimated relationship between malaria prevalence for children aged 2-10 and monthly cumulative precipitation and are plotted relative to a month with no rainfall. All relationships are estimated for contemporaneous monthly precipitation. All standard errors are clustered at the first administrative unit (e.g., province) level.

Region	**Scenario**	**2048-2052**		**2096-2100**	
		Estimate	**95% CI**	**Estimate**	**95% CI**
Sub-Saharan Africa (continent-wide)	SSP1-RCP2.6	-0.0856	(-0.411, 0.169)	-0.0942	(-0.497, 0.160)
	SSP2-RCP4.5	-0.148	(-0.570, 0.204)	-0.433	(-1.371, 0.249)
	SSP5-RCP8.5	-0.244	(-0.803, 0.261)	-1.89	(-4.846, -0.065)
East Africa	SSP1-RCP2.6	0.112	(-0.179, 0.466)	0.0984	(-0.248, 0.449)
	SSP2-RCP4.5	0.131	(-0.268, 0.543)	0.131	(-0.577, 0.846)
	SSP5-RCP8.5	0.157	(-0.371, 0.688)	-0.603	(-2.715, 0.951)
Central Africa	SSP1-RCP2.6	-0.0346	(-0.354, 0.205)	-0.0605	(-0.430, 0.242)
	SSP2-RCP4.5	-0.0212	(-0.471, 0.385)	-0.231	(-1.192, 0.514)
	SSP5-RCP8.5	-0.109	(-0.690, 0.444)	-1.43	(-4.361, 0.371)
Southern Africa	SSP1-RCP2.6	0.321	(-0.094, 0.836)	0.339	(-0.062, 0.925)
	SSP2-RCP4.5	0.507	(-0.055, 1.104)	0.844	(-0.185, 1.940)
	SSP5-RCP8.5	0.846	(-0.079, 1.810)	0.492	(-2.313, 2.547)
West Africa	SSP1-RCP2.6	-0.448	(-0.952, -0.135)	-0.449	(-1.087, 0.065)
	SSP2-RCP4.5	-0.694	(-1.290, -0.232)	-1.51	(-3.045, -0.481)
	SSP5-RCP8.5	-1.04	(-1.860, -0.358)	-4.25	(-8.780, -1.519)

Table S1: **Projected future impacts of climate change on $Pf\mathbf{PR}_{2-10}$.** Estimates and confidence intervals are all given as percentage point changes from a 2015-2020 baseline, estimated across 10,000 simulations.

	Dependent variable:								
	$Pf\text{PR}_{2-10}$								
	cnty + yr + mo FEs. (1)	cnty trd, mo FEs. (2)	cnty trd, cnty-mo FEs. (3)	cnty trd, int + mo FEs. (4)	cnty trd, int + rgn-mo FEs. (5)	cnty trd, int + cnty-mo FEs. (6)	rgn-yr + rgn-mo FEs. (7)	rgn-yr + cnty-mo FEs. (8)	rgn-yr+rgn-mo FEs., cnty trd (9)
Avg temp. (°C)	2.42***	3.08***	3.80***	3.23***	4.15***	3.97***	3.13***	2.11	3.06***
	(0.83)	(0.88)	(1.39)	(0.87)	(1.08)	(1.39)	(1.00)	(1.34)	(0.99)
Avg temp.2 (°C)	−0.06***	−0.07***	−0.07***	−0.07***	−0.08***	−0.08***	−0.07***	−0.05*	−0.06***
	(0.02)	(0.02)	(0.03)	(0.02)	(0.02)	(0.03)	(0.02)	(0.03)	(0.02)
Flood	−0.76	−0.37	−0.73	−0.27	−0.27	−0.65	−0.88	−1.15	−0.82
	(0.75)	(0.74)	(0.82)	(0.74)	(0.78)	(0.82)	(0.76)	(0.80)	(0.74)
Flood (lag 1)	−0.56	−0.40	−0.50	−0.46	−0.46	−0.55	−0.77	−1.09	−0.57
	(0.73)	(0.76)	(0.85)	(0.75)	(0.76)	(0.83)	(0.73)	(0.80)	(0.72)
Flood (lag 2)	1.68***	1.52**	2.03***	1.69***	1.71**	2.19***	2.13***	1.94***	1.79***
	(0.65)	(0.65)	(0.72)	(0.65)	(0.68)	(0.72)	(0.68)	(0.72)	(0.67)
Flood (lag 3)	0.58	0.90	1.89**	0.87	0.96	1.91**	0.08	0.74	0.38
	(0.69)	(0.71)	(0.80)	(0.71)	(0.74)	(0.81)	(0.70)	(0.77)	(0.68)
Drought	0.56	0.87	−0.48	0.84	0.09	−0.57	−0.35	−0.69	−0.13
	(0.81)	(0.74)	(0.82)	(0.74)	(0.77)	(0.83)	(0.81)	(0.86)	(0.74)
Drought (lag 1)	−1.01	−1.02	−1.39	−0.92	−1.28	−1.34	−1.62**	−1.28	−1.33*
	(0.75)	(0.77)	(0.86)	(0.78)	(0.80)	(0.86)	(0.76)	(0.85)	(0.77)
Drought (lag 2)	−0.97	−1.08*	−0.88	−1.04	−1.16*	−0.95	−1.18*	−0.85	−1.24*
	(0.68)	(0.65)	(0.76)	(0.65)	(0.68)	(0.76)	(0.69)	(0.77)	(0.67)
Drought (lag 3)	0.06	0.16	0.36	0.06	0.19	0.15	−0.06	0.11	−0.16
	(0.71)	(0.73)	(0.81)	(0.73)	(0.74)	(0.80)	(0.77)	(0.83)	(0.75)
Intvn. 1955-69					−4.80***	−5.01***			
					(1.27)	(1.35)			
Intvn. 2000-15					−3.35**	−3.88**			
					(1.61)	(1.64)			
Observations	9,875	9,875	9,875	9,875	9,875	9,875	9,875	9,875	9,875
R^2	0.52	0.52	0.56	0.53	0.53	0.57	0.56	0.60	0.59
Adjusted R^2	0.48	0.49	0.51	0.49	0.49	0.51	0.52	0.53	0.54

Table S2: **Sensitivity of estimated effects of temperature and rainfall on $Pf\text{PR}_{2-10}$ to alternative spatiotemporal controls.** All columns show regression results for a dependent variable of malaria prevalence for children aged 2-10 ($Pf\text{PR}_{2-10}$). All include fixed effects (i.e., dummy variables) at the scale of the first administrative unit (i.e., ADM1). Other model controls by column are: (1) country, year, and month fixed effects; (2) country-specific quadratic time trends and month fixed effects; (3) country-specific quadratic time trends and country-by-month fixed effects; (4) country-specific quadratic time trends and intervention period and month fixed effects; (5) country-specific quadratic time trends and intervention period and region-by-month fixed effects; (6) country-specific quadratic time trends and intervention period and country-by-month fixed effects; (7) region-by-year and region-by-month fixed effects; (8) region-by-year and country-by-month fixed effects; (9) and region-by-year and region-by-month fixed effects and country-specific linear time trends. The preferred specification used throughout the main text is column (5). In columns (5) and (7)-(9), "region" refers to the Global Burden of Disease regional definitions of western, southern, central, and eastern Africa. All standard errors are clustered at the first administrative unit (e.g., province) level.

References

1. Romanello, M, Di Napoli, C, Drummond, P, Green, C, Kennard, H, Lampard, P, Scamman, D, Arnell, N, Ayeb-Karlsson, S, Ford, L. B, et al. (2022) The 2022 report of the lancet countdown on health and climate change: health at the mercy of fossil fuels. *The Lancet* **400**, 1619–1654.

2. Ebi, K. L, Åström, C, Boyer, C. J, Harrington, L. J, Hess, J. J, Honda, Y, Kazura, E, Stuart-Smith, R. F, & Otto, F. E. (2020) Using detection and attribution to quantify how climate change is affecting health: Study explores detection and attribution to examine how climate change is affecting health. *Health Affairs* **39**, 2168–2174.

3. Carlson, C. J, Lukas-Sithole, M, Shumba, D. S, North, M, Lippi, C, Gibb, R, Carleton, T, Chersich, M, Lavelle, T, Mitchell, D, New, M, Ryan, S. J, & Trisos, C. H. (2024) Detection and attribution of climate change impacts on human health: A data science framework. *Wellcome Open Research* **9**, 245.

4. Snow, R. W, Sartorius, B, Kyalo, D, Maina, J, Amratia, P, Mundia, C. W, Bejon, P, & Noor, A. M. (2017) The prevalence of *Plasmodium falciparum* in sub-Saharan Africa since 1900. *Nature* **550**, 515–518.

5. Alcayna, T, Fletcher, I, Gibb, R, Tremblay, L, Funk, S, Rao, B, & Lowe, R. (2022) Climate-sensitive disease outbreaks in the aftermath of extreme climatic events: a scoping review. *One Earth* **5**, 336–350.

6. Mordecai, E. A, Paaijmans, K. P, Johnson, L. R, Balzer, C, Ben-Horin, T, de Moor, E, McNally, A, Pawar, S, Ryan, S. J, Smith, T. C, et al. (2013) Optimal temperature for malaria transmission is dramatically lower than previously predicted. *Ecology Letters* **16**, 22–30.

7. Mordecai, E. A, Caldwell, J. M, Grossman, M. K, Lippi, C. A, Johnson, L. R, Neira, M, Rohr, J. R, Ryan, S. J, Savage, V, Shocket, M. S, et al. (2019) Thermal biology of mosquito-borne disease. *Ecology Letters* **22**, 1690–1708.

8. Villena, O. C, Ryan, S. J, Murdock, C. C, & Johnson, L. R. (2022) Temperature impacts the environmental suitability for malaria transmission by anopheles gambiae and anopheles stephensi. *Ecology* p. e3685.

9. Ryan, S. J, McNally, A, Johnson, L. R, Mordecai, E. A, Ben-Horin, T, Paaijmans, K, & Lafferty, K. D. (2015) Mapping physiological suitability limits for malaria in Africa under climate change. *Vector-Borne and Zoonotic Diseases* **15**, 718–725.

10. Ryan, S. J, Lippi, C. A, & Zermoglio, F. (2020) Shifting transmission risk for malaria in Africa with climate change: a framework for planning and intervention. *Malaria Journal* **19**, 1–14.

11. Caminade, C, McIntyre, K. M, & Jones, A. E. (2019) Impact of recent and future climate change on vector-borne diseases. *Annals of the New York Academy of Sciences* **1436**, 157–173.

12. Murdock, C, Sternberg, E, & Thomas, M. (2016) Malaria transmission potential could be reduced with current and future climate change. *Scientific Reports* **6**, 1–7.

13. Yamana, T. K, Bomblies, A, & Eltahir, E. A. (2016) Climate change unlikely to increase malaria burden in West Africa. *Nature Climate Change* **6**, 1009–1013.

14. Loevinsohn, M. E. (1994) Climatic warming and increased malaria incidence in rwanda. *The Lancet* **343**, 714–718.

15. Ezzati, M, Lopez, A. D, Rodgers, A. A, & Murray, C. J. (2004) *Comparative quantification of health risks: global and regional burden of disease attributable to selected major risk factors*. (World Health Organization).

16. Hay, S. I, Rogers, D. J, Randolph, S. E, Stern, D. I, Cox, J, Shanks, G. D, & Snow, R. W. (2002) Hot topic or hot air? Climate change and malaria resurgence in East African highlands. *Trends in Parasitology* **18**, 530–534.

17. Alsop, Z. (2007) Malaria returns to Kenya's highlands as temperatures rise. *The Lancet* **370**, 925–926.

18. Shanks, G. D, Hay, S. I, Omumbo, J. A, & Snow, R. W. (2005) Malaria in kenya's western highlands. *Emerging infectious diseases* **11**, 1425.

19. Gething, P. W, Smith, D. L, Patil, A. P, Tatem, A. J, Snow, R. W, & Hay, S. I. (2010) Climate change and the global malaria recession. *Nature* **465**, 342–345.

20. Zhou, G, Minakawa, N, Githeko, A. K, & Yan, G. (2004) Association between climate variability and malaria epidemics in the east african highlands. *Proceedings of the National Academy of Sciences* **101**, 2375–2380.

21. Pascual, M, Ahumada, J. A, Chaves, L. F, Rodo, X, & Bouma, M. (2006) Malaria resurgence in the East African highlands: temperature trends revisited. *Proceedings of the National Academy of Sciences* **103**, 5829–5834.

22. Pascual, M, Cazelles, B, Bouma, M, Chaves, L, & Koelle, K. (2008) Shifting patterns: malaria dynamics and rainfall variability in an african highland. *Proceedings of the Royal Society B: Biological Sciences* **275**, 123–132.

23. Omumbo, J. A, Lyon, B, Waweru, S. M, Connor, S. J, & Thomson, M. C. (2011) Raised temperatures over the kericho tea estates: revisiting the climate in the east african highlands malaria debate. *Malaria Journal* **10**, 1–16.

24. Alonso, D, Bouma, M. J, & Pascual, M. (2010) Epidemic malaria and warmer temperatures in recent decades in an East African highland. *Proceedings of the Royal Society B: Biological Sciences* **278**, 1661–1669.

25. Hay, S. I, Myers, M. F, Burke, D. S, Vaughn, D. W, Endy, T, Ananda, N, Shanks, G. D, Snow, R. W, & Rogers, D. J. (2000) Etiology of interepidemic periods of mosquito-borne disease. *Proceedings of the National Academy of Sciences* **97**, 9335–9339.

26. Shanks, G, Biomndo, K, Hay, S, & Snow, R. (2000) Changing patterns of clinical malaria since 1965 among a tea estate population located in the kenyan highlands. *Transactions of the Royal Society of Tropical Medicine and Hygiene* **94**, 253–255.

27. Shanks, G. D, Hay, S. I, Stern, D. I, Biomndo, K, & Snow, R. W. (2002) Meteorologic influences on plasmodium falciparum malaria in the highland tea estates of kericho, western kenya. *Emerging infectious diseases* **8**, 1404.

28. Hay, S. I, Cox, J, Rogers, D. J, Randolph, S. E, Stern, D. I, Shanks, G. D, Myers, M. F, & Snow, R. W. (2002) Climate change and the resurgence of malaria in the East African highlands. *Nature* **415**, 905.

29. Hay, S. I, Shanks, G. D, Stern, D. I, Snow, R. W, Randolph, S. E, & Rogers, D. J. (2005) Climate variability and malaria epidemics in the highlands of east africa. *Trends in parasitology* **21**, 52–53.

30. Stern, D. I, Gething, P. W, Kabaria, C. W, Temperley, W. H, Noor, A. M, Okiro, E. A, Shanks, G. D, Snow, R. W, & Hay, S. I. (2011) Temperature and malaria trends in highland east africa. *PloS one* **6**, e24524.

31. Krsulovic, F. A. M, Moulton, T. P, Lima, M, & Jacksic, F. (2021) Epidemic malaria dynamics in eastern africa highlands: the role of climate change and human population growth. *Ecol Evolut Bio* **6**, 23–30.

32. Chaves, L. F & Koenraadt, C. J. (2010) Climate change and highland malaria: fresh air for a hot debate. *The Quarterly review of biology* **85**, 27–55.

33. Siraj, A, Santos-Vega, M, Bouma, M, Yadeta, D, Carrascal, D. R, & Pascual, M. (2014) Altitudinal changes in malaria incidence in highlands of Ethiopia and Colombia. *Science* **343**, 1154–1158.

34. Rodó, X, Martinez, P. P, Siraj, A, & Pascual, M. (2021) Malaria trends in Ethiopian highlands track the 2000 'slowdown' in global warming. *Nature Communications* **12**, 1–12.

35. Ruiz, D, Brun, C, Connor, S. J, Omumbo, J. A, Lyon, B, & Thomson, M. C. (2014) Testing a multi-malaria-model ensemble against 30 years of data in the kenyan highlands. *Malaria Journal* **13**, 1–14.

36. Pörtner, H.-O, Roberts, D. C, Adams, H, Adler, C, Aldunce, P, Ali, E, Begum, R. A, Betts, R, Kerr, R. B, Biesbroek, R, et al. (2022) *Climate Change 2022: Impacts, adaptation and vulnerability*. (IPCC Geneva, Switzerland:).

37. Callahan, C. W & Mankin, J. S. (2022) National attribution of historical climate damages. *Climatic Change* **172**, 40.

38. Swain, D. L, Singh, D, Touma, D, & Diffenbaugh, N. S. (2020) Attributing extreme events to climate change: a new frontier in a warming world. *One Earth* **2**, 522–527.

39. Stott, P. A, Christidis, N, Otto, F. E, Sun, Y, Vanderlinden, J.-P, van Oldenborgh, G. J, Vautard, R, von Storch, H, Walton, P, Yiou, P, et al. (2016) Attribution of extreme weather and climate-related events. *Wiley Interdisciplinary Reviews: Climate Change* **7**, 23–41.

40. Otto, F. E. (2017) Attribution of weather and climate events. *Annual Review of Environment and Resources* **42**, 627–646.

41. Noy, I, Stone, D, & Uher, T. (2024) Extreme events impact attribution: A state of the art. *Cell Reports Sustainability* **1**.

42. Carlson, C. J, Mitchell, D, Carleton, T, Chersich, M, Gibb, R, Lavelle, T, Lukas-Sithole, M, North, M, Lippi, C, New, M, et al. (2024) Designing and describing climate change impact attribution studies: a guide to common approaches.

43. Ebi, K. L, Ogden, N. H, Semenza, J. C, & Woodward, A. (2017) Detecting and attributing health burdens to climate change. *Environmental Health Perspectives* **125**, 085004.

44. Burke, M, González, F, Baylis, P, Heft-Neal, S, Baysan, C, Basu, S, & Hsiang, S. (2018) Higher temperatures increase suicide rates in the United States and Mexico. *Nature Climate Change* **8**, 723–729.

45. Carleton, T. A & Hsiang, S. M. (2016) Social and economic impacts of climate. *Science* **353**.

46. Organization, W. H et al. (2022) *World malaria report 2022*. (World Health Organization).

47. Hsiang, S. (2016) Climate econometrics. *Annual Review of Resource Economics* **8**, 43–75.

48. Carleton, T, Jina, A, Delgado, M, Greenstone, M, Houser, T, Hsiang, S, Hultgren, A, Kopp, R. E, McCusker, K. E, Nath, I, et al. (2022) Valuing the global mortality consequences of climate change accounting for adaptation costs and benefits. *The Quarterly Journal of Economics* **137**, 2037–2105.

49. Smith, M. W, Willis, T, Mroz, E, James, W. H, Klaar, M. J, Gosling, S. N, & Thomas, C. J. (2024) Future malaria environmental suitability in africa is sensitive to hydrology. *Science* **384**, 697–703.

50. Adeola, A. M, Botai, J. O, Rautenbach, H, Adisa, O. M, Ncongwane, K. P, Botai, C. M, & Adebayo-Ojo, T. C. (2017) Climatic variables and malaria morbidity in mutale local municipality, south africa: a 19-year data analysis. *International journal of environmental research and public health* **14**, 1360.

51. Lindsay, S. W, Bødker, R, Malima, R, Msangeni, H. A, & Kisinza, W. (2000) Effect of 1997–98 ei niño on highland malaria in tanzania. *The Lancet* **355**, 989–990.

52. Teklehaimanot, H. D, Lipsitch, M, Teklehaimanot, A, & Schwartz, J. (2004) Weather-based prediction of plasmodium falciparum malaria in epidemic-prone regions of ethiopia i. patterns of lagged weather effects reflect biological mechanisms. *Malaria journal* **3**, 1–11.

53. Boyce, R, Reyes, R, Matte, M, Ntaro, M, Mulogo, E, Metlay, J. P, Band, L, & Siedner, M. J. (2016) Severe flooding and malaria transmission in the western ugandan highlands: implications for disease control in an era of global climate change. *The Journal of infectious diseases* **214**, 1403–1410.

54. Paaijmans, K. P, Wandago, M. O, Githeko, A. K, & Takken, W. (2007) Unexpected high losses of anopheles gambiae larvae due to rainfall. *PloS one* **2**, e1146.

55. Govoetchan, R, Gnanguenon, V, Azondékon, R, Agossa, R. F, Sovi, A, Oké-Agbo, F, Ossè, R, & Akogbéto, M. (2014) Evidence for perennial malaria in rural and urban areas under the sudanian climate of kandi, northeastern benin. *Parasites & Vectors* **7**, 1–12.

56. Smith, M, Macklin, M, & Thomas, C. (2013) Hydrological and geomorphological controls of malaria transmission. *Earth-Science Reviews* **116**, 109–127.

57. Mouchet, J, Manguin, S, Sircoulon, J, Laventure, S, Faye, O, Onapa, A, Carnevale, P, Julvez, J, & Fontenille, D. (1998) Evolution of malaria in africa for the past 40 years: impact of climatic and human factors. *Journal of the American Mosquito Control Association* **14**, 121–130.

58. Schultz, K. A & Mankin, J. S. (2019) Is temperature exogenous? the impact of civil conflict on the instrumental climate record in sub-saharan africa. *American Journal of Political Science* **63**, 723–739.

59. Auffhammer, M, Hsiang, S. M, Schlenker, W, & Sobel, A. (2011) Global climate models and climate data: a user guide for economists. *Unpublished manuscript* **1**, 10529–10530.

60. Mordecai, E. A, Ryan, S. J, Caldwell, J. M, Shah, M. M, & LaBeaud, A. D. (2020) Climate change could shift disease burden from malaria to arboviruses in africa. *The Lancet Planetary Health* **4**, e416–e423.

61. Feachem, R. G, Chen, I, Akbari, O, Bertozzi-Villa, A, Bhatt, S, Binka, F, Boni, M. F, Buckee, C, Dieleman, J, Dondorp, A, et al. (2019) Malaria eradication within a generation: ambitious, achievable, and necessary. *The Lancet* **394**, 1056–1112.

62. Tian, H, Li, N, Li, Y, Kraemer, M. U, Tan, H, Liu, Y, Li, Y, Wang, B, Wu, P, Cazelles, B, et al. (2022) Malaria elimination on Hainan Island despite climate change. *Communications Medicine* **2**, 1–9.

63. Jaramillo-Ochoa, R, Sippy, R, Farrell, D. F, Cueva-Aponte, C, Beltrán-Ayala, E, Gonzaga, J. L, Ordoñez-León, T, Quintana, F. A, Ryan, S. J, & Stewart-Ibarra, A. M. (2019) Effects of political instability in Venezuela on malaria resurgence at Ecuador–Peru border, 2018. *Emerging Infectious Diseases* **25**, 834.

64. Walker, P. G, White, M. T, Griffin, J. T, Reynolds, A, Ferguson, N. M, & Ghani, A. C. (2015) Malaria morbidity and mortality in Ebola-affected countries caused by decreased health-care capacity, and the potential effect of mitigation strategies: a modelling analysis. *The Lancet Infectious Diseases* **15**, 825–832.

65. Miazgowicz, K, Shocket, M, Ryan, S, Villena, O, Hall, R, Owen, J, Adanlawo, T, Balaji, K, Johnson, L, Mordecai, E, et al. (2020) Age influences the thermal suitability of *Plasmodium falciparum* transmission in the Asian malaria vector *Anopheles stephensi*. *Proceedings of the Royal Society B* **287**, 20201093.

66. Sinka, M, Pironon, S, Massey, N, Longbottom, J, Hemingway, J, Moyes, C, & Willis, K. (2020) A new malaria vector in africa: Predicting the expansion range of anopheles stephensi and identifying the urban populations at risk. *Proceedings of the National Academy of Sciences* **117**, 24900–24908.

67. Ryan, S. J, Lippi, C. A, Villena, O. C, Singh, A. H, Murdock, C. C, & Johnson, L. R. (2022) Mapping current and future thermal limits to suitability for malaria transmission by the invasive mosquito anopheles stephensi. *bioRxiv* pp. 2022–12.

68. Harris, I, Osborn, T. J, Jones, P, & Lister, D. (2020) Version 4 of the cru ts monthly high-resolution gridded multivariate climate dataset. *Scientific data* **7**, 1–18.

69. Gidden, M, Riahi, K, Smith, S, Fujimori, S, Luderer, G, Kriegler, E, van Vuuren, D. P, van den Berg, M, Feng, L, Klein, D, et al. (2019) Global emissions pathways under different socioeconomic scenarios for use in CMIP6: a dataset of harmonized emissions trajectories through the end of the century. *Geoscientific Model Development Discussions* **12**, 1443–1475.

70. O'Neill, B. C, Tebaldi, C, Van Vuuren, D. P, Eyring, V, Friedlingstein, P, Hurtt, G, Knutti, R, Kriegler, E, Lamarque, J.-F, Lowe, J, et al. (2016) The Scenario Model Intercomparison Project (ScenarioMIP) for CMIP6. *Geoscientific Model Development* **9**, 3461–3482.

71. Van Vuuren, D. P, Kriegler, E, O'Neill, B. C, Ebi, K. L, Riahi, K, Carter, T. R, Edmonds, J, Hallegatte, S, Kram, T, Mathur, R, et al. (2014) A new scenario framework for climate change research: scenario matrix architecture. *Climatic Change* **122**, 373–386.

72. Kriegler, E, Bauer, N, Popp, A, Humpenöder, F, Leimbach, M, Strefler, J, Baumstark, L, Bodirsky, B. L, Hilaire, J, Klein, D, et al. (2017) Fossil-fueled development (SSP5): an energy and resource intensive scenario for the 21st century. *Global Environmental Change* **42**, 297–315.

73. Fricko, O, Havlik, P, Rogelj, J, Klimont, Z, Gusti, M, Johnson, N, Kolp, P, Strubegger, M, Valin, H, Amann, M, et al. (2017) The marker quantification of the Shared Socioeconomic Pathway 2: A middle-of-the-road scenario for the 21st century. *Global Environmental Change* **42**, 251–267.

74. Cannon, A. J, Sobie, S. R, & Murdock, T. Q. (2015) Bias correction of GCM precipitation by quantile mapping: How well do methods preserve changes in quantiles and extremes? *Journal of Climate* **28**, 6938–6959.

75. Cayan, D. R, Maurer, E. P, Dettinger, M. D, Tyree, M, & Hayhoe, K. (2008) Climate change scenarios for the California region. *Climatic Change* **87**, 21–42.

76. Artzy-Randrup, Y, Alonso, D, & Pascual, M. (2010) Transmission intensity and drug resistance in malaria population dynamics: implications for climate change. *PloS one* **5**, e13588.

77. Laneri, K, Paul, R. E, Tall, A, Faye, J, Diene-Sarr, F, Sokhna, C, Trape, J.-F, & Rodó, X. (2015) Dynamical malaria models reveal how immunity buffers effect of climate variability. *Proceedings of the National Academy of Sciences* **112**, 8786–8791.

78. Cervellati, M, Esposito, E, & Sunde, U. (2022) Epidemic shocks and civil violence: Evidence from malaria outbreaks in africa. *The Review of Economics and Statistics* **104**, 780–796.

79. Schlenker, W & Roberts, M. J. (2009) Nonlinear temperature effects indicate severe damages to us crop yields under climate change. *Proceedings of the National Academy of sciences* **106**, 15594–15598.

80. Hsiang, S. M, Meng, K. C, & Cane, M. A. (2011) Civil conflicts are associated with the global climate. *Nature* **476**, 438–441.

81. Deschênes, O & Greenstone, M. (2007) The economic impacts of climate change: evidence from agricultural output and random fluctuations in weather. *American economic review* **97**, 354–385.

82. Kipruto, E. K, Ochieng, A. O, Anyona, D. N, Mbalanya, M, Mutua, E. N, Onguru, D, Nyamongo, I. K, & Estambale, B. (2017) Effect of climatic variability on malaria trends in baringo county, kenya. *Malaria journal* **16**, 1–11.

819 83. Moran, A. E, Oliver, J. T, Mirzaie, M, Forouzanfar, M. H, Chilov, M, Anderson, L,
820 Morrison, J. L, Khan, A, Zhang, N, Haynes, N, et al. (2012) Assessing the global
821 burden of ischemic heart disease: part 1: methods for a systematic review of the
822 global epidemiology of ischemic heart disease in 1990 and 2010. *Global Heart* **7**,
823 315–329.

824 84. Mabaso, M. L, Craig, M, Ross, A, & Smith, T. (2007) Environmental predictors
825 of the seasonality of malaria transmission in africa: the challenge. *The American*
826 *journal of tropical medicine and hygiene* **76**, 33–38.

827 85. Bhatt, S, Weiss, D, Cameron, E, Bisanzio, D, Mappin, B, Dalrymple, U, Battle,
828 K, Moyes, C, Henry, A, Eckhoff, P, et al. (2015) The effect of malaria control on
829 *Plasmodium falciparum* in Africa between 2000 and 2015. *Nature* **526**, 207–211.

830 86. Li, C & Managi, S. (2022) Global malaria infection risk from climate change. *Envi-*
831 *ronmental Research* **214**, 114028.